JGR Solid Earth

RESEARCH ARTICLE

10.1029/2021JB022437

Key Points:

- $MgFeO_{2.5}$, $FeFeO_3$, and total Fe^{3+} contents in bridgmanite decrease with increasing pressure
- Fe^{3+}-linked oxygen vacancies in bridgmanite are destabilized by increasing pressure
- $MgFeO_{2.5}$ can be formed in Fe^{3+}-rich bridgmanite under the topmost lower mantle conditions

Supporting Information:

Supporting Information may be found in the online version of this article.

Correspondence to:

H. Fei,
hongzhan.fei@uni-bayreuth.de

Citation:

Fei, H., Liu, Z., Huang, R., Kamada, S., Hirao, N., Kawaguchi, S., et al. (2021). Pressure destabilizes oxygen vacancies in bridgmanite. *Journal of Geophysical Research: Solid Earth*, *126*, e2021JB022437. https://doi.org/10.1029/2021JB022437

Received 17 MAY 2021
Accepted 16 NOV 2021

Pressure Destabilizes Oxygen Vacancies in Bridgmanite

Hongzhan Fei[1], Zhaodong Liu[1,2], Rong Huang[1,3], Seiji Kamada[4,5], Naohisa Hirao[6], Saori Kawaguchi[6], Catherine McCammon[1], and Tomoo Katsura[1,7]

[1]Bayerisches Geoinstitut, University of Bayreuth, Bayreuth, Germany, [2]State Key Laboratory of Superhard Materials, Jilin University, Changchun, China, [3]Department of Earth Sciences, University College London, London, UK, [4]Frontier Research Institute for Interdisciplinary Sciences, Tohoku University, Sendai, Japan, [5]Department of Earth Science, Tohoku University, Sendai, Japan, [6]Japan Synchrotron Radiation Research Institute (JASRI), Sayo, Japan, [7]Center for High Pressure Science and Technology Advanced Research, Beijing, China

Abstract

Bridgmanite may contain a large proportion of ferric iron in its crystal structure in the forms of $FeFeO_3$ and $MgFeO_{2.5}$ components. We investigated the pressure dependence of $FeFeO_3$ and $MgFeO_{2.5}$ contents in bridgmanite coexisting with $MgFe_2O_4$-phase and with or without ferropericlase in the MgO-SiO_2-Fe_2O_3 ternary system at 2,300 K, 33 and 40 GPa. Together with the experiments at 27 GPa reported in Fei et al. (2020, https://doi.org/10.1029/2019GL086296), our results show that the $FeFeO_3$ and $MgFeO_{2.5}$ contents in bridgmanite decrease from 7.6 to 5.3 mol % and from 2 to 3 mol % to nearly zero, respectively, with increasing pressure from 27 to 40 GPa. Accordingly, the total Fe^{3+} decreases from 0.18 to 0.11 pfu. The formation of oxygen vacancies ($MgFeO_{2.5}$ component) in bridgmanite is therefore dramatically suppressed by pressure. Oxygen vacancies can be produced by ferric iron in Fe^{3+}-rich bridgmanite under the topmost lower mantle conditions, but the concentration should decrease rapidly with increasing pressure. The variation of oxygen-vacancy content with depth may potentially affect the physical properties of bridgmanite and thus affect mantle dynamics.

Plain Language Summary

Bridgmanite is the most abundant mineral in the Earth's lower mantle. Although its basic chemical formula is $MgSiO_3$, large amounts of Fe^{3+} can be added in the following two ways: (1) Two Fe^{3+} replace Mg^{2+} and Si^{4+} and form the $FeFeO_3$ component. This is called charge-coupled substitution because the overall charge does not change. (2) One Fe^{3+} replaces one Si^{4+} and forms the $MgFeO_{2.5}$ component. Here the loss of positive charge is compensated by a loss of oxygen and is therefore called oxygen-vacancy substitution. In this study, we measured the effect of pressure on the abundance of these two components of bridgmanite. We found that the $MgFeO_{2.5}$ content decreases greatly with increasing pressure. Some oxygen sites may therefore be vacant in bridgmanite at the top of lower mantle, but the concentration of oxygen vacancies should decrease rapidly in deeper regions. The decrease of oxygen-vacancy concentration in bridgmanite will change the nature of the lower mantle, for example, rocks will become harder, and electrical conductivity will decrease with increasing depth.

1. Introduction

It is known that the disproportionation reaction of iron from Fe^{2+} to Fe^{3+} and Fe^0 can occur in Earth's deep lower mantle (Armstrong et al., 2019; Frost et al., 2004). In particular, the separation of metallic iron and Fe^{3+}-bearing silicate magma during core formation would raise the $Fe^{3+}/\Sigma Fe$ ratio in silicate magma, resulting in high proportion of Fe^{3+} in deep mantle minerals that precipitated from the magma ocean (e.g., Andrault et al., 2018; Armstrong et al., 2019; Boujibar et al., 2016; Frost et al., 2008). On the other hand, the redox-induced density contrast may produce locally Fe^{3+}-rich regions (Gu et al., 2016), whereas slabs may transport oxidized components into the deep mantle by subduction (Zhao et al., 2021). Therefore, it is expected that minerals in the deep mantle may contain large amount of Fe^{3+} ($Fe^{3+}/\Sigma Fe$ up to 60% or more), at least locally (e.g., Armstrong et al., 2019; Bindi et al., 2020; Boujibar et al., 2016; Frost et al., 2004; Grocholski et al., 2009; Gu et al., 2016; Jackson et al., 2005; Kupenko et al., 2015; Kurnosov et al., 2017; Lauterbach et al., 2000; Li et al., 2006; McCammon, 1997; Piet et al., 2016; Prescher et al., 2014; Shim et al., 2017; Sinmyo et al., 2011), although they are under relatively reducing conditions with oxygen fugacity close to the iron-wüstite buffer (Frost & McCammon, 2008). Since Fe^{3+} may affect the chemical and physical properties of minerals by changing their defect chemistry (e.g., Creasy et al., 2020; Fei et al., 1994; Glazyrin et al., 2014; Holzapfel et al., 2005; Liu et al., 2018; Sinmyo et al., 2019;

Wang et al., 2021), knowledge of mineral phase relations in Fe^{3+}-rich systems is critical for investigating the structure, dynamics, and evolution of Earth's mantle.

Bridgmanite is stabilized in the pressure range 23–125 GPa (e.g., Ishii et al., 2018; Murakami et al., 2004) and is the dominant mineral in Earth (e.g., Irifune & Ringwood, 1987a, 1987b). It can incorporate large amounts of trivalent elements such as Al^{3+} and Fe^{3+} in its crystal structure (e.g., Andrault et al., 1998; McCammon, 1997; Navrotsky, 1999; Navrotsky et al., 2003; Shim et al., 2017) by the formation of XXO_3 and $MgXO_{2.5}$ components (X is Fe^{3+} or Al^{3+}) via charge-coupled and oxygen-vacancy mechanisms, respectively (e.g., Huang, Boffa-Ballaran, McCammon, Miyajima, Dolejš & Frost, 2021; Huang, Boffa-Ballaran, McCammon, Miyajima, & Frost, 2021; Lauterbach et al., 2000; Liu, Akaogi, & Katsura, 2019; Liu, Ishii, & Katsura, 2017; Liu, Boffa-Ballaran, et al., 2019; Liu et al., 2020; Navrotsky, 1999; Navrotsky et al., 2003; Nishio-Hamane et al., 2005, 2008; O'Neill & Jeanloiz, 1994). The different substitution mechanisms thus produce different types of defect species. The defect-controlled physical properties of bridgmanite such as atomic diffusivity, elasticity, plasticity, and electrical conductivity will depend on the substitution mechanisms (e.g., Andrault et al., 2007, 2001; Boffa-Ballaran et al., 2012; Brodholt, 2000; Creasy et al., 2020; Daniel et al., 2004; Frost & Langenhorst, 2002; Saikia et al., 2009; Xu et al., 1998; Yagi et al., 2004; Yoshino et al., 2016; Zhang & Weidner, 1999).

The Al^{3+} substitution mechanism in Fe^{3+}-free bridgmanite has been systematically studied (e.g., Andrault et al., 1998; Brodholt, 2000; Grüninger et al., 2019; Kojitani, Katsura, & Akaogi, 2007; Liu, Akaogi, & Katsura, 2019; Liu, Ishii, & Katsura, 2017; Liu, Boffa-Ballaran, et al., 2019; Navrotsky et al., 2003; Panero et al., 2006; Stebbins et al., 2003; Walter et al., 2004, 2006; Yamamoto et al., 2003). It has been found that the $MgAlO_{2.5}$ component is formed in MgO-excess systems, but not in SiO_2-excess systems (Liu, Akaogi, & Katsura, 2019; Liu, Boffa-Ballaran, et al., 2019). The concentration of $AlAlO_3$ increases with pressure and temperature, whereas the $MgAlO_{2.5}$ content increases with temperature but decreases with pressure (Brodholt, 2000; Liu, Ishii, & Katsura, 2017; Liu, Nishi, et al., 2017; Liu, Akaogi, & Katsura, 2019).

In contrast to Al^{3+} substitution, the Fe^{3+} substitution mechanism in bridgmanite has been less studied. The majority of previous studies focused on Fe^{3+}-Al^{3+} coupling (e.g., Frost & Langenhorst, 2002; Liu, Dubrovinsky, et al., 2019; Liu et al., 2020; Mohn & Trønnes, 2016; Nishio-Hamane et al., 2005; Richmond & Brodholt, 1998; Saikia et al., 2009; Vanpeteghem et al., 2006; Walter et al., 2004), and only a few studies examined Fe^{3+} substitution in Fe^{3+}-rich systems. Earlier studies regarding Fe^{3+} substitution in Fe^{3+}-rich bridgmanite show a dominance of the charge-coupled substitution mechanism (Andrault & Bolfan-Casanova, 2001; Catalli et al., 2010). However, recent studies with well-constrained chemical compositions (Fei et al., 2020; Huang, Boffa-Ballaran, McCammon, Miyajima, Dolejš & Frost, 2021; Hummer & Fei, 2012; Sinmyo et al., 2014) show that bridgmanite can contain 2–3 mol % of the $MgFeO_{2.5}$ component in addition to the $FeFeO_3$ component in the presence of ferropericlase at 25–27 GPa, that is, relatively low-pressure conditions of the bridgmanite stability field. It was also demonstrated that the $FeFeO_3$ content increases with increasing temperature, whereas the $MgFeO_{2.5}$ content is independent of temperature (Fei et al., 2020). However, the pressure dependence of Fe^{3+} substitution in bridgmanite is still unclear.

In this study, we investigated the substitution mechanism of Fe^{3+} in Al^{3+}-free bridgmanite using a recently developed ultrahigh-pressure (>25 GPa) multianvil technique with tungsten carbide anvils (Ishii et al., 2016, 2019) at 33 and 40 GPa at 2300 K. Although bridgmanite in the lower mantle contains Al^{3+}, which could affect the Fe^{3+} substitution as mentioned above, we investigated the Al^{3+}-free system to provide basic understanding of the roles of trivalent cations in bridgmanite chemistry. To maximize the $MgFeO_{2.5}$ content in bridgmanite, experiments were performed in the MgO-SiO_2-Fe_2O_3 system where bridgmanite coexists with $MgFe_2O_4$-phase, and with/without ferropericlase. Together with our recent work at 27 GPa (Fei et al., 2020), we show that the concentrations of both $FeFeO_3$ and $MgFeO_{2.5}$ in bridgmanite, and thus the total Fe^{3+} content, decrease with increasing pressure. Even coexisting with ferropericlase, the formation of oxygen vacancies is completely suppressed at about 40 GPa. Our results provide basic knowledge about the phase relations and Fe^{3+} substitution mechanisms in bridgmanite under Fe^{3+}-rich conditions.

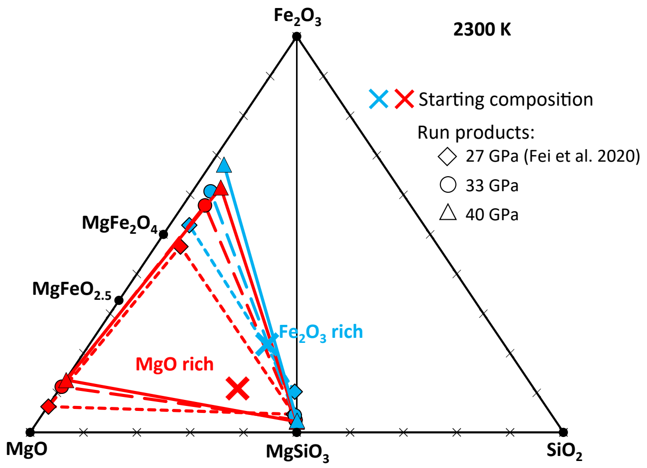

Figure 1. Chemical compositions of MgO-rich and Fe_2O_3-rich starting materials and run products in the ternary phase diagram with endmembers of Fe_2O_3, MgO, and SiO_2. The 27 GPa run was already reported in Fei et al. (2020).

2. Experimental Procedure

2.1. High-Pressure Multianvil Experiments

The starting materials used in this study were identical to those in Fei et al. (2020), that is, mixtures with compositions of 5MgO +3SiO_2 + 1Fe_2O_3 (MgO-rich sample) and 4MgO + 3SiO_2 + 2Fe_2O_3 (Fe_2O_3-rich sample) prepared from SiO_2, MgO, and Fe_2O_3 oxides (Figure 1). The purity of each oxide was >99.9%. Platinum chambers with inner diameter of 0.3 mm, outer diameter of 0.4 mm, and length of 0.3 mm were used as sample capsules, which were placed in a Al_2O_3 sleeve in the $LaCrO_3$ furnace. A Cr_2O_3-doped MgO octahedron with edge length of 5.7 mm was used as the pressure medium (Figure 2).

High pressures were generated by tungsten carbide anvils with truncation edge lengths of 1.5 mm using the 15 MN multianvil press, IRIS-15, at the University of Bayreuth (Ishii et al., 2016). The experimental pressures were 33 and 40 GPa (Table 1). The temperature and annealing duration were 2,300 K and 24 hr, respectively. After annealing, the heating power supplier was switched off, by which the temperature decreased to less than 800 K within 1 s and to less than 400 K within 2–4 s. Afterward, the pressure was decreased to ambient conditions over durations exceeding 15 hr.

2.2. Sample Analysis

(1) *Scanning Electron Microscopy (SEM)*. Cross sections of the recovered assemblies were prepared and analyzed by SEM. Backscattered electron images (BSE) were taken on the cross sections (Figure 3). The presented phases on the cross sections were examined by an energy dispersive detector

(2) *X-ray Diffraction*. Microfocus X-ray diffraction analyses were performed using a microfocus X-ray diffractometer (Brucker AXS D8 Discover) with a microfocus source of Co-Kα radiation. The beam diameter was about 100 μm focused on the cross sections of the recovered samples. The acceleration voltage and beam current were 40 kV and 500 μA, respectively. The exposure time was 5–6 hr for each analysis. Examples of the diffraction patterns are shown in Figure 4

(3) *Mössbauer Spectroscopy*. Synchrotron Mössbauer source (SMS) spectroscopy analyses were performed under ambient conditions on all the samples at beamline BL10XU, SPring-8, Japan. The detailed setup and analytical conditions of SMS spectroscopy are given in Hirao et al. (2020). The spectra were fitted using MossA with Lorentzian doublets (Prescher et al., 2012) (Figure 5)

(4) *Electron Microprobe Analysis*. The chemical compositions of bridgmanite and coexisting phases were obtained by electron probe microanalyzer (EPMA) at the University of Bayreuth. The acceleration voltage was 15 kV, the beam current was 5 nA, and the counting time was 20 s for each point analysis. An enstatite standard was used for Mg and Si, whereas metallic iron was used for Fe. Tests were also made using a Fe_2O_3-standard for analysis of Fe in the samples, which did not show any meaningful difference compared to results using a metallic-Fe standard. Grains near the Pt capsule wall were avoided in the analyses

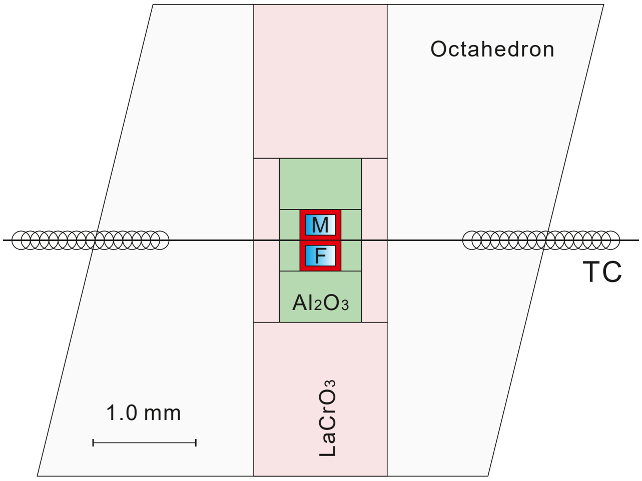

Figure 2. Design of the 5.7/1.5 multianvil cell assembly for 33 and 40 GPa runs. M: MgO-rich starting material. F: Fe_2O_3-rich starting material.

2.3. Calculation of Chemical Formula

Assuming that $MgSiO_3 + MgFeO_{2.5} + FeFeO_3 = 100\%$ in the recovered bridgmanite samples, the molar concentrations of the three components were obtained from the equation (Grüninger et al., 2019; Liu, Ishii, & Katsura, 2017),

Table 1
List of Run Conditions and Chemical Compositions of the Run Products

														Bridgmanite (mol %)			$MgFe_2O_4$-phase (mol %)			Ferropericlase (mol %)	
Starting material	Run. No.	Assembly	*P* (GPa)	*T* (h)	Phase	*N*	MgO wt%	SiO_2 wt%	Fe_2O_3 wt%	Total wt%	Mg pfu	Si pfu	Fe pfu	$FeFeO_3$	$MgFeO_{2.5}$	$MgSiO_3$	Mg_2SiO_4	$MgFe_2O_4$	$Fe_{8/3}O_4$	MgO	FeO
MgO-rich	I574 (Fei et al., 2020)	7/3	27	9	Bridgmanite	17	35.94 (99)	52.29 (80)	13.47 (42)	101.70 (123)	0.923 (15)	0.902 (13)	0.175 (7)	7.6 (15)	2.2 (27)	90.2 (13)	–	–	–	–	–
					$MgFe_2O_4$	11	19.82 (34)	2.85 (9)	76.25 (95)	98.92 (119)	0.957 (9)	0.093 (3)	1.858 (10)	–	–	–	9.5 (3)	78.3 (15)	12.2 (13)	–	–
					(Mg·Fe)O	7	89.75 (117)	0.25 (17)	11.17 (36)	101.16 (85)	0.932 (5)	0.002 (1)	0.065 (3)	–	–	–	–	–	–	93.5 (5)	6.5 (3)
	I873	5.7/1.5	33	24	Bridgmanite	16	36.38 (81)	53.68 (99)	9.34 (98)	99.40 (88)	0.944 (11)	0.934 (11)	0.122 (14)	5.6 (13)	1.0 (20)	93.4 (11)	–	–	–	–	–
					$MgFe_2O_4$	16	13.78 (25)	2.20 (22)	81.17 (66)	97.14 (75)	0.716 (11)	0.077 (7)	2.130 (14)	–	–	–	7.6 (7)	55.4 (21)	37.1 (15)		
					(Mg·Fe)O	11	79.57 (235)	0.20 (19)	20.60 (53)	100.37 (261)	0.882 (5)	0.002 (1)	0.115 (2)	–	–	–	–	–	–	88.4 (3)	11.6 (3)
	I909	5.7/1.5	40	24	Bridgmanite	24	37.67 (66)	56.14 (103)	8.31 (59)	102.12 (134)	0.947 (13)	0.947 (11)	0.106 (8)	5.3 (13)	0.0 (23)	94.7 (11)	–	–	–	–	–
					$MgFe_2O_4$	14	11.70 (60)	2.52 (43)	85.94 (102)	102.40 (41)	0.584 (26)	0.084 (14)	2.165 (34)	–	–	–	8.4 (14)	41.5 (18)	50.1 (18)	–	–
					(Mg·Fe)O	17	78.49 (56)	0.21 (56)	23.69 (32)	102.40 (41)	0.812 (6)	0.001 (4)	0.124 (2)	–	–	–	–	–	–	86.8 (1)	13.2 (1)
Fe_2O_3-rich	I574 (Fei et al., 2020)	7/3	27	9	Bridgmanite	15	29.72 (94)	43.57 (194)	26.67 (211)	99.96 (170)	0.821 (18)	0.807 (25)	0.372 (36)	17.9 (18)	1.4 (26)	80.7 (25)	–	–	–		–
					$MgFe_2O_4$	13	16.98 (37)	2.11 (7)	79.99 (50)	99.09 (67)	0.846 (14)	0.071 (2)	2.013 (12)	–	–	–	7.1 (2)	70.4 (17)	22.5 (16)	–	–
	I646 (Fei et al., 2020)	7/3	27	20	Bridgmanite	9	31.45 (94)	46.78 (126)	23.40 (246)	101.63 (67)	0.843 (19)	0.841 (18)	0.316 (35)	15.7 (19)	0.2 (13)	84.1 (18)	–	–	–	–	–
					$MgFe_2O_4$	9	18.23 (50)	4.55 (23)	74.25 (137)	97.04 (140)	0.8W85 (19)	0.148 (8)	1.819 (26)	–	–	–	15.1 (8)	60.2 (22)	24.7 (21)	–	–
	I873	5.7/1.5	33	24	Bridgmanite	20	35.50 (83)	52.10 (97)	12.58 (142)	100.18 (95)	0.924 (13)	0.910 (11)	0.166 (20)	7.6 (13)	1.4 (14)	91.0 (11)	–	–	–	–	–
					$MgFe_2O_4$	13	12.37 (21)	1.75 (7)	83.57 (92)	97.69 (83)	0.652 (11)	0.062 (3)	2.224 (13)	–	–	–	6.0 (3)	51.4 (12)	42.6 (12)	–	–
	I909	5.7/1.5	40	24	Bridgmanite	14	37.35 (100)	55.81 (80)	9.07 (84)	102.23 (99)	0.941 (16)	0.944 (12)	0.115 (12)	5.9 (16)	−0.2 (26)	94.4 (12)	–	–	–	–	–
					$MgFe_2O_4$	13	9.90 (67)	1.5 (21)	88.93 (102)	100.07 (45)	0.502 (33)	0.042 (7)	2.276 (27)	–	–	–	4.2 (7)	41.7 (31)	54.1 (31)	–	–

Note. All experiments were performed at 2,300 K. Runs I574 and I646 at 27 GPa are already reported in Fei et al. (2020). *P*: pressure. *t*: annealing time. *N*: number of analyzed points by electron microprobe. The error bars are one standard deviation of *N* points from electron microprobe analysis.

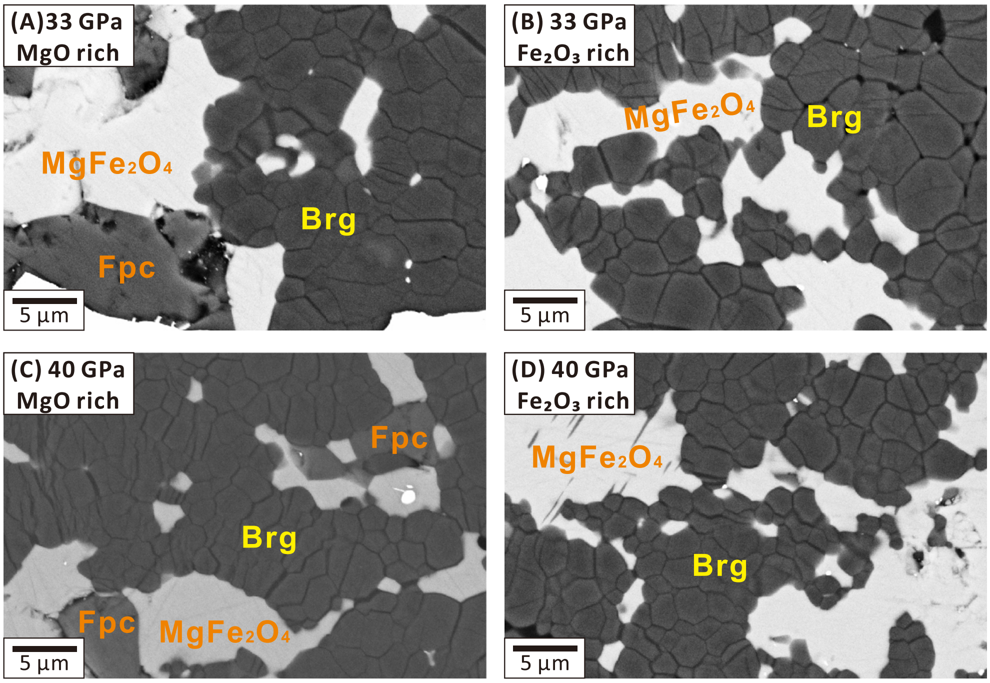

Figure 3. SEM images of samples recovered from 33 (a, b) and 40 GPa (c, d). Brg: bridgmanite. Fpc: ferropericlase. $MgFe_2O_4$: $MgFe_2O_4$-phase.

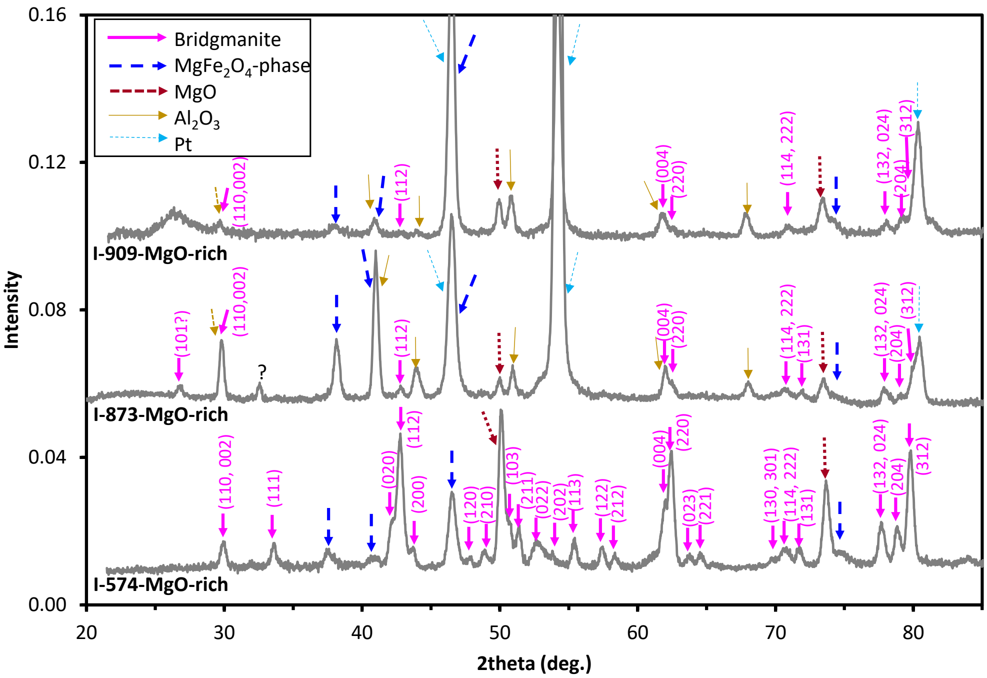

Figure 4. X-ray diffraction spectra of the recovered samples (MgO-rich conditions). Pt and Al_2O_3 peaks are from the sample capsule and the sleeve outside of the capsule in the cell assembly (Figure 2), respectively, owing to the limited spatial resolution of the diffractometer. The $MgFe_2O_4$-phase show consistent peaks at different pressures, indicting the same structure. The spectra are background subtracted. The identified peaks of bridgmanite are labeled in the figure (hkl), and their d-spacings and fitted lattice parameters are given in the online Supporting Information (Table S1).

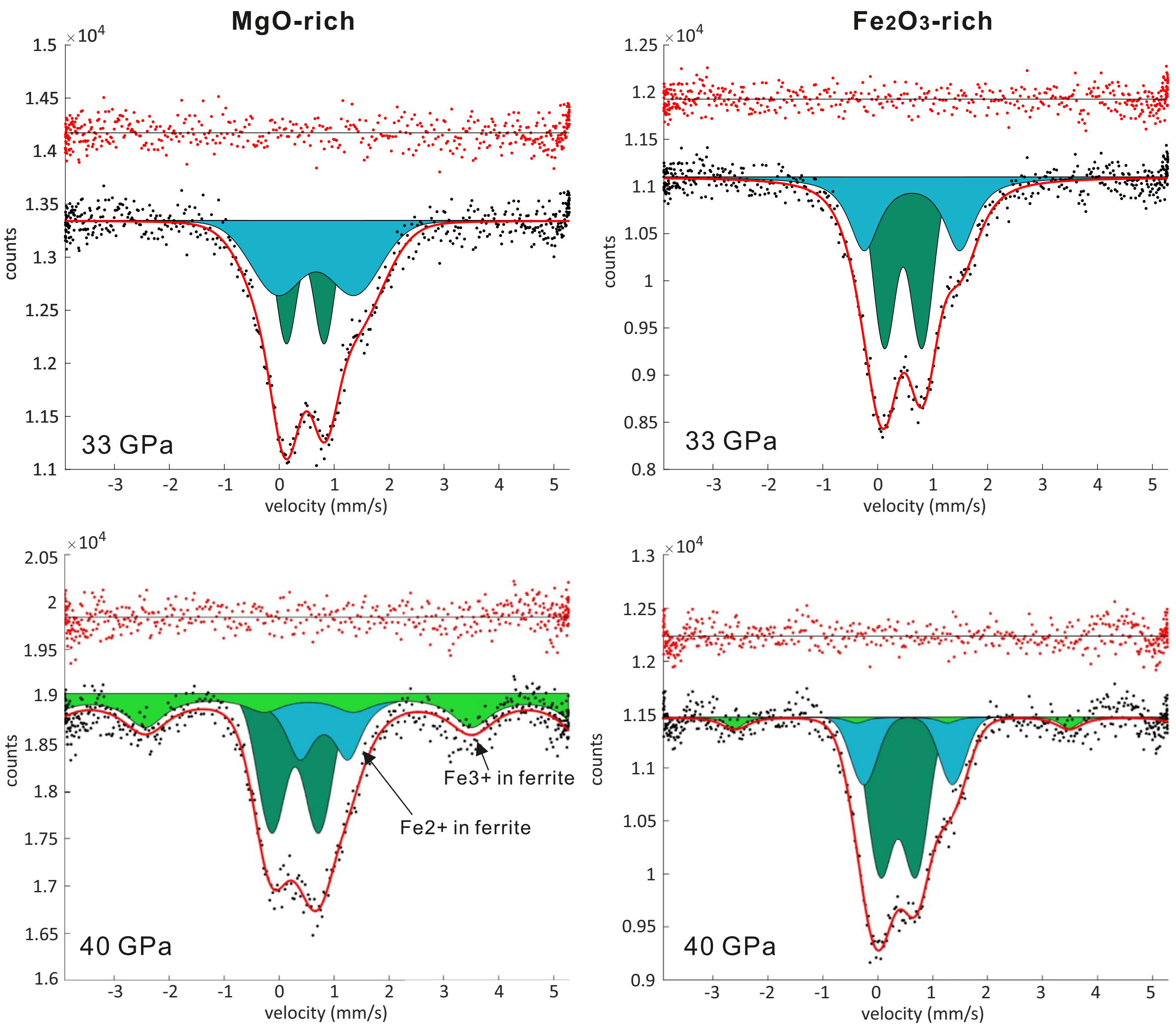

Figure 5. Synchrotron Mössbauer source spectra of the recovered samples. Left: MgO-rich samples. Right: Fe_2O_3-rich samples. A baseline was subtracted from the raw spectra determined from a calibration using the single-line absorber $K_2Mg^{57}Fe(CN)_6$. The dark green doublets correspond to Fe^{3+} in bridgmanite, the blue doublets are Fe^{3+} or $Fe^{2.5+}$ in nonmagnetic $MgFe_2O_4$-phase, and the light green doublets are Fe^{3+} in magnetic $MgFe_2O_4$-phase.

$$Mg_aFe_bSi_cO_{a+1.5b+2c} = cMgSiO_3 + (a-c)MgFeO_{2.5} + \frac{b-a+c}{2}FeFeO_3 \quad (1)$$

where the atomic ratio of Mg, Fe, and Si (a: b: c) in bridgmanite was taken from EPMA. The presence of an $MgFeO_{2.5}$ component can be indicated by higher Mg atomic content than Si ($a > c$), whereas there should be no $MgFeO_{2.5}$ component if $a = c$. The Mg content could be lower than Si ($a < c$) if Fe^{3+} is partially reduced, which is not the case in this study since $Fe^{3+}/\Sigma Fe \approx 100\%$ based on Mössbauer analysis as described later.

Similarly, the concentrations of $MgFe_2O_4$, Mg_2SiO_4, and $Fe_{8/3}O_4$ components in the $MgFe_2O_4$-phase were calculated from the EPMA results by assuming $Fe^{3+}/\Sigma Fe \approx 100\%$, whereas MgO and FeO components in ferropericlase were calculated by assuming all Fe as ferrous (Table 1).

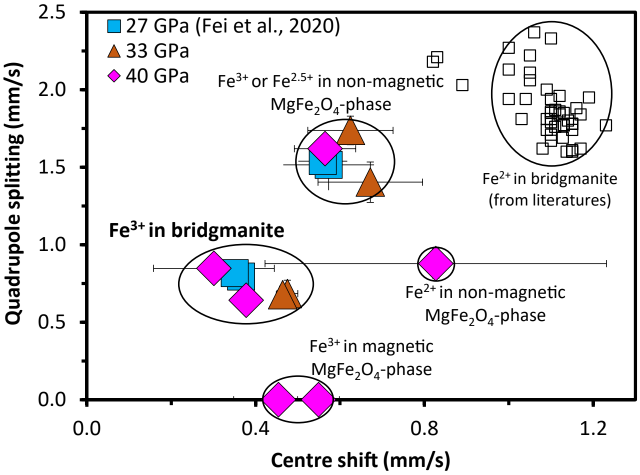

Figure 6. Center shift and quadrupole splitting derived from fits of the Mössbauer spectra. There is no detectable Fe^{2+} in bridgmanite, which should have center shift and quadrupole splitting of about 0.9–1.2 and 1.5–2.5 mm/s, respectively, based on the literature data as shown by open squares (Huang, Boffa-Ballaran, McCammon, Miyajima, Dolejš & Frost, 2021; Lauterbach et al., 2000; McCammon, 1998; Sinmyo et al., 2019).

3. Experimental Results

3.1. Phase Assemblages in the Recovered Samples

The recovered MgO-rich and Fe_2O_3-rich samples contain bridgmanite, a phase close to $MgFe_2O_4$ composition (hereafter $MgFe_2O_4$-phase), and either with (MgO-rich samples) or without (Fe_2O_3-rich samples) ferropericlase (Table 1 and Figure 1), as demonstrated by the backscattering images (Figure 3) and X-ray diffraction (Figure 4). No observable inhomogeneity of phase compositions was found throughout the capsules, indicating that chemical equilibrium was reached.

The $MgFe_2O_4$-phase was previously assigned to be a $CaMn_2O_4$-type structure (Andrault & Bolfan-Casanova, 2001; Fei et al., 2020) or $CaTi_2O_4$-type structure (Greenberg et al., 2017), and recently suggested to be a new structure (modified Na-Fe-Ti oxide-type) of post-spinel (Ishii et al., 2020). Our study primarily focused on the bridgmanite phase without considering the structural complexities of the $MgFe_2O_4$-phase.

3.2. $Fe^{3+}/\Sigma Fe$ in the Run Products

Mössbauer spectra unambiguously indicate the predominance of Fe^{3+} in bridgmanite (Figures 5 and 6). Although fitting models are not unique due to the high degree of line overlap, the Fe^{2+} in bridgmanite as $Fe^{2+}SiO_3$ component, whose hyperfine parameters are expected to have center shift (CS) and quadrupole splitting (QS) of 0.9–1.2 and 1.5–2.5 mm/s, respectively (e.g., Huang, Boffa-Ballaran, McCammon, Miyajima, Dolejš & Frost, 2021; Hummer & Fei, 2012; Lauterbach et al., 2000; McCammon, 1998; Sinmyo et al., 2019), was not detected in any plausible fit. Instead, doublets of Fe^{3+} or $Fe^{2.5+}$ in nonmagnetic $MgFe_2O_4$-phase were identified in the run products from all high-pressure conditions, whereas Fe^{2+} in nonmagnetic $MgFe_2O_4$-phase and Fe^{3+} in magnetic $MgFe_2O_4$-phase were fitted in the 40 GPa samples (Figures 5 and 6). Because of the small proportion of ferropericlase, doublets of ferropericlase are not observed within the experimental data scatter.

3.3. Composition of Bridgmanite, $MgFe_2O_4$-Phase, and Ferropericlase

By comparison of bridgmanite compositions at 33 and 40 GPa with that at 27 GPa from Fei et al. (2020), it is found that the Fe^{3+} content in bridgmanite under MgO-rich conditions decreases dramatically from ∼0.17 pfu at 27 GPa (Fei et al., 2020) to ∼0.11 pfu at 40 GPa (Figure 7a). As expected, the Fe_2O_3-rich samples have higher Fe^{3+} content than the MgO-rich samples, and Fe^{3+} content decreases from 0.37 to 0.12 pfu at 27–40 GPa (Figure 7a). The Mg/Si ratios in bridgmanite are slightly higher than unity in the MgO-rich samples, whereas they are essentially unity in the Fe_2O_3-rich samples (Table 1).

The composition of the $MgFe_2O_4$-phase deviates from the $MgFe_2O_4$ endmember (Figure 1). With increasing pressure from 27 to 40 GPa, the Fe^{3+} content increases from 1.9 to 2.3 pfu, and the Mg content decreases from 0.9 to 0.5 pfu. The Si content is low but detectable (∼0.1 pfu) (Figure 7b). Additionally, up to 13.2 mol % Fe was found in ferropericlase (Figure 7c).

4. Discussion

4.1. Fe^{3+} and Fe^{2+} Partitioning Between Bridgmanite and Ferropericlase

The Fe contents [Fe/(Fe + Mg)] in ferropericlase of the MgO-rich samples are 6.5–13.2% (Figure 7c). If all Fe were ferrous in ferropericlase, the partition coefficient of Fe^{2+} between bridgmanite and ferropericlase would be nearly zero based on the absence of Fe^{2+} in the current bridgmanite samples. The partition coefficient is thus much smaller than that suggested by previous studies (e.g., Nakajima et al., 2012; Prescher et al., 2014; Xu et al., 2017), who reported values of 0.2–0.4 at 25–40 GPa. We emphasize that this discrepancy cannot be caused by undetectable Fe^{2+} in our bridgmanite samples. If the Fe^{2+}/Mg partition coefficient given by previous

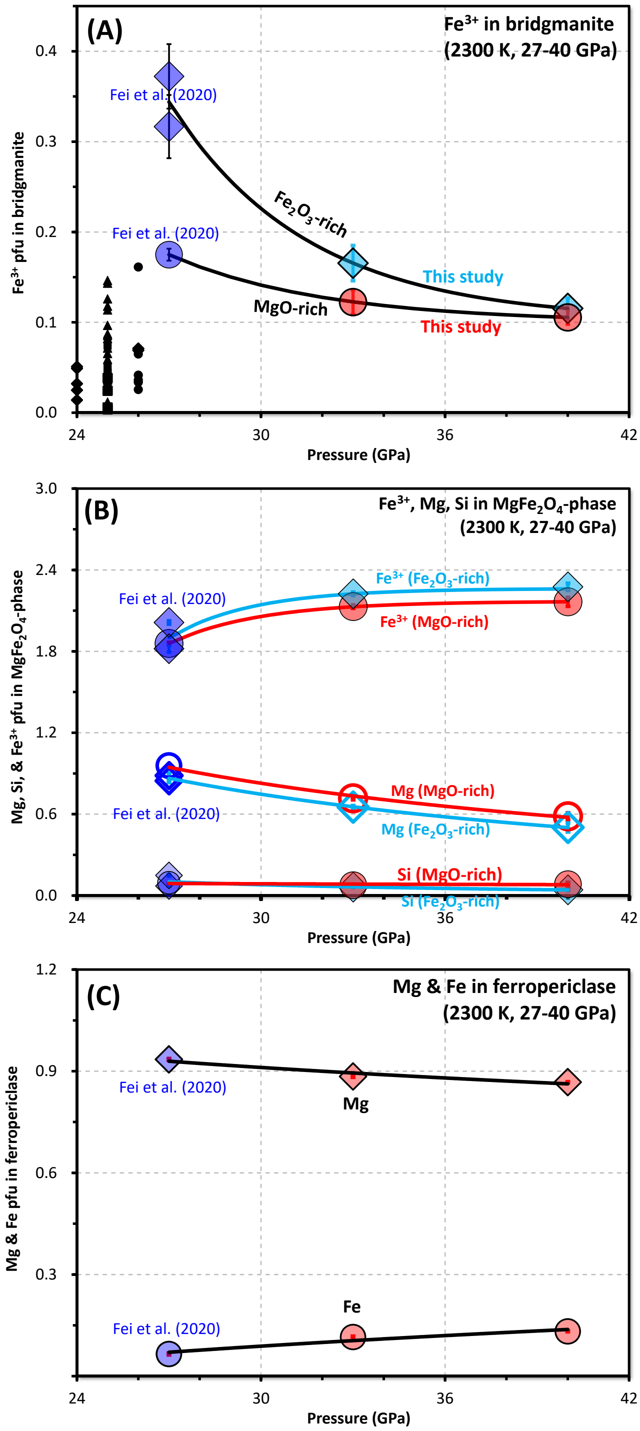

Figure 7. Chemical composition of bridgmanite, ferropericlase, and $MgFe_2O_4$-phase in run products. (a) Fe^{3+} content in bridgmanite calculated to O = 3. (b) Mg, Si, and Fe^{3+} contents in the $MgFe_2O_4$-phase calculated to O = 4. (c) Mg and Fe content in ferropericlase from MgO-rich samples calculated to O = 1 assuming that all Fe is ferrous in ferropericlase. Black symbols represent the Fe^{3+} content in bridgmanite that coexists with ferropericlase reported in previous studies (Frost & Langenhorst, 2002; Frost et al., 2004; Huang, Boffa-Ballaran, McCammon, Miyajima, Dolejš & Frost, 2021; Hummer & Fei, 2012; Lauterbach et al., 2000), all of which are lower than this study because their experimental temperatures are lower, and/or $MgFe_2O_4$-phase did not appear (namely Fe^{3+} is not saturated). The data points with blue symbols at 27 GPa are from Fei et al. (2020). The error bars represent one standard deviation of the analyzed points by electron microprobe as shown in Table 1.

studies were followed by our samples, $Fe^{2+}/\Sigma Fe$ should be 15–50% in bridgmanite. Such a significant fraction of Fe^{2+} would definitely be detectable by both in-house (Fei et al., 2020) and synchrotron (this study) Mössbauer spectroscopy because the hyperfine parameters of Fe^{2+} doublets in bridgmanite are well known and would not overlap with other components in our spectra (e.g., Huang, Boffa-Ballaran, McCammon, Miyajima, Dolejš & Frost, 2021; Sinmyo et al., 2019; Yoshino et al., 2016, Figure 6). Therefore, the appearance of 6.5–13.2 mol % FeO in ferropericlase does not suggest the presence of Fe^{2+} in bridgmanite. Since the experiments in previous studies (e.g., Nakajima et al., 2012; Prescher et al., 2014) were mostly performed under relatively reducing conditions with high $Fe^{2+}/\Sigma Fe$ ratios, one explanation for this discrepancy is that Fe^{2+} is almost entirely incorporated into ferropericlase when the bulk Fe^{2+} content in the system is extremely low, that is, the partition coefficient may have a substantial compositional dependence.

4.2. Fe^{3+} Content in Bridgmanite

Based on the phase rule, the Fe^{3+} content in bridgmanite under MgO-rich conditions should be uniquely constrained because three phases coexist in the system. Although some Fe_2O_3 might be reduced to FeO in high-pressure experiments as indicated by the presence of Fe in ferropericlase in MgO-rich samples (Figure 7a), the number of components in bridgmanite is still three because the $Fe^{3+}/\Sigma Fe$ ratio is close to 100% in bridgmanite as demonstrated by Mössbauer spectroscopy.

The Fe_2O_3-rich samples in this study and some other studies (e.g., Andrault & Bolfan-Casanova, 2001; Liu et al., 2018; Wang et al., 2021) show much higher Fe^{3+} contents in bridgmanite (up to 1.0 pfu) than the current MgO-rich bridgmanite samples. However, these high Fe^{3+}-content bridgmanite samples did not coexist with ferropericlase (bridgmanite + $MgFe_2O_4$-phase in Fe_2O_3-rich samples in this study and only bridgmanite in Andrault & Bolfan-Casanova, 2001, Liu et al., 2018, and Wang et al., 2021). When bridgmanite coexists with ferropericlase, the Fe^{3+} content in bridgmanite will be limited because of the formation of the $MgFe_2O_4$-phase from $FeFeO_3$ and MgO (Andrault & Bolfan-Casanova, 2001). When bridgmanite does not coexist with MgO, the Fe^{3+} content in bridgmanite depends on the starting material. If the bulk Fe^{3+} content in the starting material is high, the Fe^{3+} content in bridgmanite can accordingly be high based on the phase relations in Figure 1, for example, Fe^{3+} can reach 1.0 pfu as shown in Liu et al. (2018) and Wang et al. (2021). This is understandable because the molar volume of hematite (30.5 cm^3/mol) is slightly larger than the $FeFeO_3$ component in bridgmanite (29.55 cm^3/mol, Huang, Boffa-Ballaran, McCammon, Miyajima, & Frost, 2021). Therefore, Fe^{3+} may tend to be incorporated in bridgmanite by a $MgSiO_3$-Fe_2O_3 solid solution instead of forming hematite, consequently, the Fe^{3+} solubility in bridgmanite is high. The upper limit of Fe^{3+} content should be obtained in the system with coexistence of bridgmanite and hematite, which was not investigated in this study. Additionally, the formation of the $FeAlO_3$ component will also increase the Fe^{3+} content in Al-bearing bridgmanite, which causes the high Fe^{3+} content (about 0.7 pfu) in Liu, Dubrovinsky, et al. (2019) and Liu et al. (2020).

The $MgFe_2O_4$-phase may have structural complexities (e.g., Andrault & Bolfan-Casanova, 2001; Greenberg et al., 2017; Ishii et al., 2020), which may affect Fe^{3+} partitioning between bridgmanite and the $MgFe_2O_4$-phase and thus affect the Fe^{3+} content in bridgmanite. Some studies reported phase transitions among polymorphs of $MgFe_2O_4$ at high temperatures below 25 GPa (e.g., Ishii et al., 2020; Uenver-Thiele et al., 2017), and at ambient temperature in the pressure range 25–40 GPa (Greenberg et al., 2017). However, no phase transition of $MgFe_2O_4$ has been reported at the conditions of our experiments, that is, 2,300 K and 27–40 GPa. The absence of a phase transition of the $MgFe_2O_4$-phase in this study has also been indicated by X-ray diffraction of the recovered samples (Figure 4). Therefore, the systematic decrease of Fe^{3+} content in bridgmanite is not expected to be caused by complex polymorphism of $MgFe_2O_4$.

4.3. Pressure Dependence of Fe^{3+} Substitution in Bridgmanite

In the MgO-rich samples, the $FeFeO_3$ content in bridgmanite decreases from 7.7 to 5.3 mol %, whereas the $MgFeO_{2.5}$ content decreases from 2.2 to ∼0% at 27–40 GPa (Figure 8a). The extrapolation of data agrees well with the maximum $MgFeO_{2.5}$ content of 3.5% reported by Hummer and Fei (2012) at 25 GPa and 1,970–2,070 K (Figure 8a). In contrast, Fe_2O_3-rich samples have $FeFeO_3$ contents ranging from 17.9% to 5.9%, which is higher than the MgO-rich samples, and have $MgFeO_{2.5}$ contents that are essentially zero within error over the entire investigated pressure range (Figure 8b).

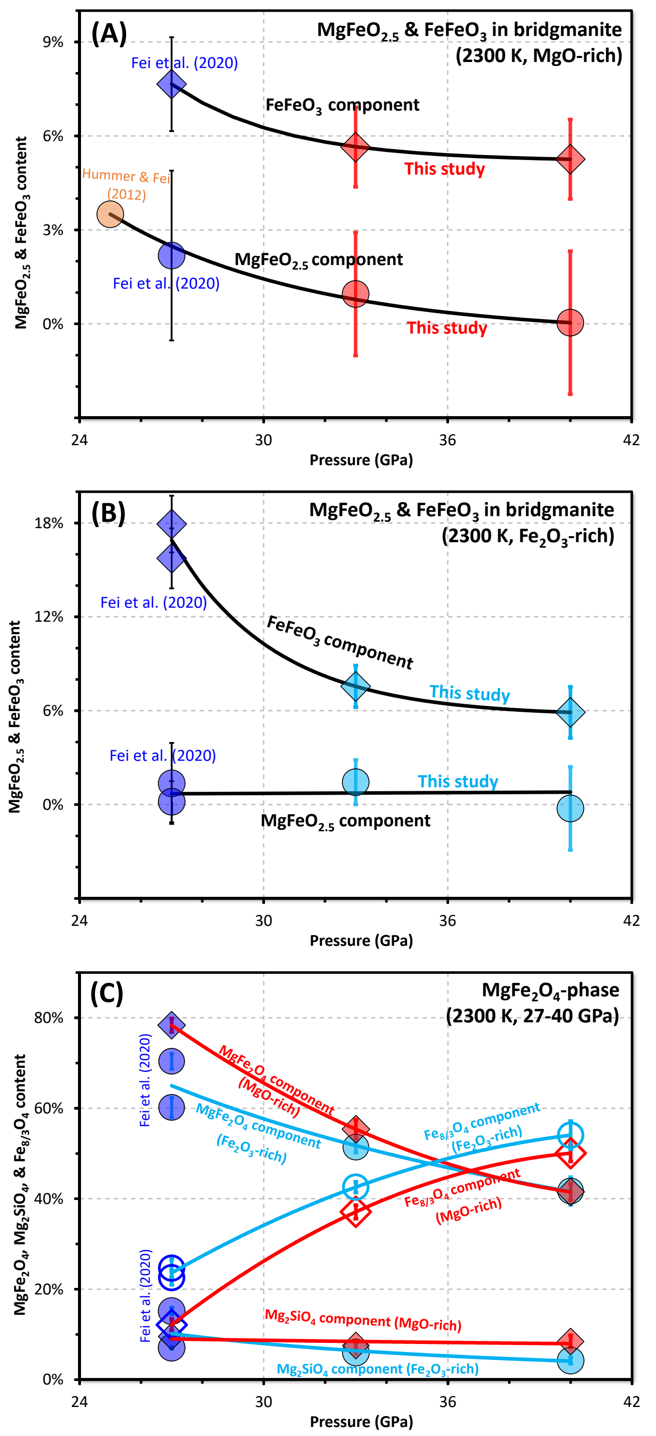

Figure 8. Substitution mechanisms in bridgmanite and $MgFe_2O_4$-phase. (a) Fe^{3+} substitution in bridgmanite under MgO-rich conditions. The maximum $MgFeO_{2.5}$ content reported by Hummer and Fei (2012) at 25 GPa, 1,970–2,070 K is also shown for comparison. (b) Fe^{3+} substitution in bridgmanite under Fe_2O_3-rich conditions. (c). Substitution mechanisms in the $MgFe_2O_4$-phase. The data points with blue symbols at 27 GPa are from Fei et al. (2020). The error bars represent one standard deviation of the analyzed points by electron microprobe as shown in Table 1.

Note that smaller Pt capsules were used in the runs at 33 and 40 GPa in this study compared to the 27 GPa runs in Fei et al. (2020). Because Pt capsules may absorb Fe from the samples and thus release O_2, more O_2 might be released in 33 and 40 GPa runs relative to sample volumes. However, the O_2 formed by Fe dissolution in Pt should not cause $MgFeO_{2.5}$ content to decrease with increasing pressure. Since $Fe^{3+}/\Sigma Fe \approx 100\%$ in bridgmanite in all runs, the chemistry of bridgmanite in MgO-rich samples is uniquely constrained with maximized Fe^{3+} content and maximized $Fe^{3+}/\Sigma Fe$ ratio. Excess O_2 cannot further oxidize bridgmanite. Therefore, the chemistry of bridgmanite from MgO-rich samples in this study will not be affected by excess O_2. Although the excess O_2 may produce peroxide components (Hu et al., 2016; Zhu et al., 2019), it requires pressures >70 GPa, which is not the case in this study.

Because of the uncertainties in the Mg, Si, and Fe contents obtained from EPMA analysis (Table 1), the error bars are relatively large for the relatively small $MgFeO_{2.5}$ contents (Figure 7a). Additionally, the reproducibility of $MgFeO_{2.5}$ content obtained in different runs under the same pressure and temperature conditions is about ±0.3–1.25 mol % (Table 1 and Fei et al., 2020), which is not negligible. These problems make it challenging to obtain a definite conclusion regarding the pressure dependence of the $MgFeO_{2.5}$ content. However, plots of Mg and Si contents in bridgmanite versus Fe^{3+} content show that data at 27 GPa and 1,700–2,300 K under MgO-rich conditions clearly deviate from the theoretical Mg and Si contents of pure $FeFeO_3$ substitution, whereas they essentially follow the trend of the pure $FeFeO_3$ substitution mechanism in Fe_2O_3-rich samples (Figure 9 and Fei et al., 2020). This behavior demonstrates the presence of $MgFeO_{2.5}$ components at 27 GPa under MgO-rich conditions. In contrast to the 27-GPa data, the 33-GPa data are closer to the pure $FeFeO_3$ substitution, and the 40-GPa data are exactly on the trend of pure $FeFeO_3$ substitution even in MgO-rich samples (Figure 9), which suggests a decrease of $MgFeO_{2.5}$ content with increasing pressure. Therefore, the reduction of $MgFeO_{2.5}$ content with increasing pressure is convincing despite relatively large uncertainties of absolute $MgFeO_{2.5}$ contents.

The suppression of Fe^{3+}-linked oxygen vacancies with increasing pressure can be understood by the volume increase associated with $MgFeO_{2.5}$ formation. Partial molar volume of the $MgFeO_{2.5}$ component in bridgmanite is estimated to be 27.65 cm^3/mol (Huang, Boffa-Ballaran, McCammon, Miyajima, & Frost, 2021), whereas the molar volume of the $MgFe_2O_4$-phase is 41.4 cm^3/mol (Ishii et al., 2020), and that of MgO is 11.25 cm^3/mol at ambient conditions (Dorogokupets, 2010; Tange et al., 2012). Thus, the volume change in the reaction,

$$\begin{aligned} & MgFe_2O_4(MgFe_2O_4\text{-phase}) + MgO\ \ (\text{periclase}) \\ & \quad = 2MgFeO_{2.5}(\text{bridgmanite}) \end{aligned} \tag{2}$$

is about +2.7 cm^3/mol at ambient conditions. This volume change will be even larger (4.3–4.7 cm^3/mol) by adjusting the pressure to 27–40 GPa using reported equation of states (Dorogokupets, 2010; Ishii et al., 2020; Tange et al., 2012), because the $MgFe_2O_4$-phase has a much smaller bulk modulus (164 GPa) than bridgmanite (257 GPa) (Ishii et al., 2020; Tange et al., 2012). The reaction should thus be significantly suppressed by increasing pressure. As a result, the concentration of $MgFeO_{2.5}$ content decreases rapidly with increasing pressure.

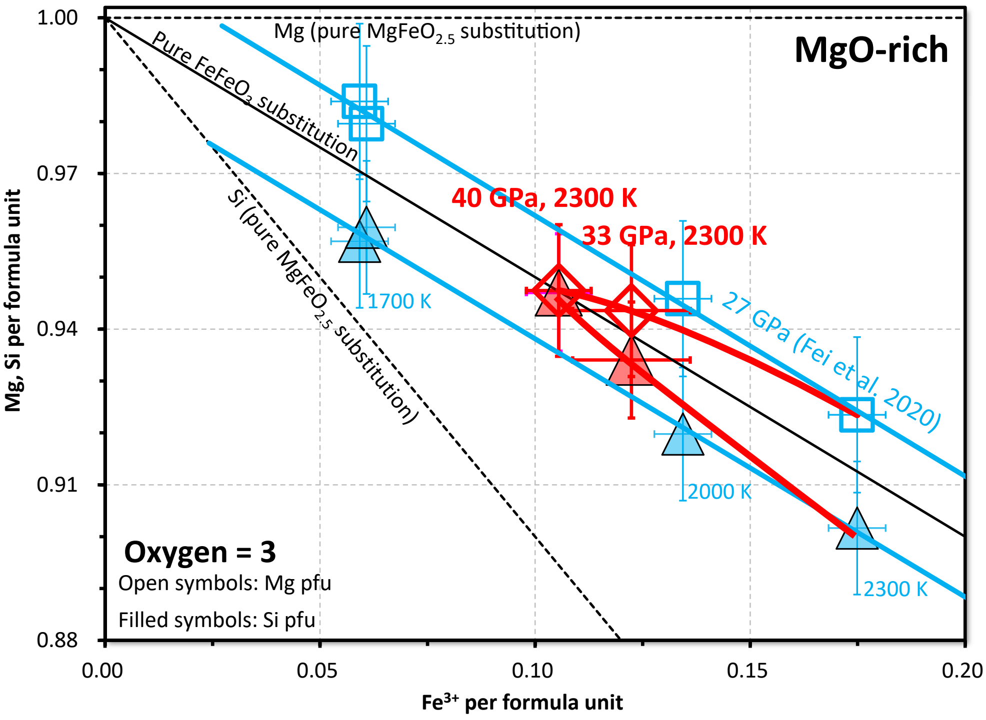

Figure 9. Mg and Si contents (per formula unit) as a function of Fe^{3+} content in bridgmanite in MgO-rich samples. The data points at 27 GPa are from Fei et al. (2020) at 1,700–2,300 K, whereas those at 33 and 40 GPa are from this study with a temperature condition of 2,300 K. The theoretical Mg and Si contents with pure $FeFeO_3$ substitution and pure $MgFeO_{2.5}$ substitution mechanisms are shown by thin solid and dashed lines, respectively. The error bars represent one standard deviation of the analyzed points by electron microprobe as shown in Table 1.

The negative pressure dependence of $MgFeO_{2.5}$ content is identical to that of the $MgAlO_{2.5}$ content in the MgO-SiO_2-Al_2O_3 system (Liu, Ishii, & Katsu, 2017), which can also be understood by the positive volume change of the reaction:

$$MgAl_2O_4\,(\text{CF-phase}) + MgO\,(\text{periclase}) = 2MgAlO_{2.5}\,(\text{bridgmanite}) \quad (3)$$

in which $MgAlO_{2.5}$ and $MgAl_2O_4$ have molar volume of 26.6 and 36.5 cm^3/mol, respectively (Huang, Boffa-Ballaran, McCammon, Miyajima, & Frost, 2021; Kojitani, Hisatomi, & Akaogi, 2007; Liu, Akaogi, & Katsura, 2019; Sueda et al., 2009).

The $FeFeO_3$ content in our samples decreases with increasing pressure as well. The reaction of Fe^{3+} between bridgmanite and $MgFe_2O_4$-phase can be written as:

$$MgFe_2O_4\,(MgFe_2O_4\text{-phase}) + FeFeO_3\,(\text{bridgmanite}) = MgO\,(\text{periclase}) \quad (4)$$

The $FeFeO_3$ component has a molar volume of 29.55 cm^3/mol (Huang, Boffa-Ballaran, McCammon, Miyajima, & Frost, 2021). Although the volume change of the above reaction is negative at ambient conditions ($\Delta V = -0.6$ cm^3/mol), it becomes positive (+0.5 to +0.8 cm^3/mol) after adjusting to 27–40 GPa using the equation of state for each phase (Dorogokupets, 2010; Ishii et al., 2020; Tange et al., 2012). As a result, the $FeFeO_3$ content in bridgmanite decreases with pressure.

In contrast to the $FeFeO_3$ component in bridgmanite, the $AlAlO_3$ content in Fe^{3+}-free bridgmanite increases with increasing pressure (Liu et al., 2016, Liu, Nishi, et al., 2017). Since bridgmanite coexists with corundum (Al_2O_3) in Liu, Ishii, and Katsura (2017) and Liu, Nishi, et al. (2017), the exchange of Al between bridgmanite and corundum can be written as:

$$Al_2O_3\,(\text{corundum}) = AlAlO_3\,(\text{bridgmanite}) \quad (5)$$

Al_2O_3 (corundum) and $AlAlO_3$ (bridgmanite) have nearly identical molar volumes (25.6 and 25.8 cm^3/mol, respectively) (Dewaele & Torrent, 2013; Huang, Boffa-Ballaran, McCammon, Miyajima, & Frost, 2021; Liu, Akaogi, & Katsura, 2019).

On the other hand, in the case that bridgmanite coexists with $MgAl_2O_4$ and MgO, the $AlAlO_3$ component in bridgmanite can be formed by,

$$MgAl_2O_4\,(\text{CF-phase}) = AlAlO_3\,(\text{bridgmanite}) + MgO\,(\text{periclase}) \tag{6}$$

which has a small, but positive volume change ($\Delta V = +0.5$ cm^3/mol at ambient conditions) using the molar volume of each component reported previously (Huang, Boffa-Ballaran, McCammon, Miyajima, & Frost, 2021; Kojitani, Hisatomi, & Akaogi, 2007; Liu, Akaogi, & Katsura, 2019; Sueda et al., 2009). Thus, the small but positive volume changes of reactions (5) and (6) suggest that the $AlAlO_3$ content in bridgmanite should slightly decrease or be nearly constant with increasing pressure, which contradicts the tendency reported by Liu et al. (2016) and Liu, Nishi, et al. (2017). A possible cause for this discrepancy could be a large uncertainty in the reported molar volume of $AlAlO_3$ component in bridgmanite since it is extrapolated from the volume of bridgmanite with relatively low $AlAlO_3$ content (up to 14 mol %) (Huang, Boffa-Ballaran, McCammon, Miyajima, & Frost, 2021; Liu, Akaogi, & Katsura, 2019; Liu, Boffa-Ballaran, et al., 2019), or that the $AlAlO_3$ component has a much smaller bulk modulus than $MgSiO_3$-bridgmanite since Al^{3+} has a smaller ionic radius than Mg^{2+} (0.50 Å versus 0.65 Å), leading to negative ΔV for reactions (5) and (6) at high pressures. In contrast, Fe^{3+} has a comparable ionic radius (0.64 Å) with Mg^{2+} and larger than Si^{4+} (0.42 Å). Therefore, the $FeFeO_3$ component should be less compressible than $AlAlO_3$ and $MgSiO_3$ components.

4.4. Chemistry of $MgFe_2O_4$-Phase

The detailed substitution mechanism of the $MgFe_2O_4$-phase is unknown, but it is assumed to be composed of $MgFe_2O_4$, $Mg2SiO_4$, and $Fe^{3+}{}_{8/3}O_3$ (or $Fe^{2+}Fe^{3+}{}_2O_4$) components (Huang, 2020; Huang, Boffa-Ballaran, McCammon, Miyajima, Dolejš & Frost, 2021; Liu, Akaogi, & Katsura, 2019). The Mg_2SiO_4 substitution mechanism occurs by replacement of two Fe^{3+} sites by Mg^{2+} and Si^{4+}. $Fe^{2+}Fe^{3+}{}_2O_4$ substitution might have occurred instead of $Fe^{3+}{}_{8/3}O_4$ if significant Fe in the $MgFe_2O_4$-phase were ferrous.

Based on the atomic contents of Mg, Si, and Fe from EPMA analysis (Table 1), the concentration of each component can be obtained by assuming the $MgFe_2O_4$-phase to be composed of $MgFe_2O_4$, Mg_2SiO_4, and $Fe_{8/3}O_4$. As shown in Figure 8c, the $Fe_{8/3}O_4$ content increases significantly from 12–25% to ∼50% with increasing pressure from 27 to 40 GPa. Correspondingly, the $MgFe_2O_4$ content decreases from 60–80% to ∼40% (Figure 8c). The variation of $Fe_{8/3}O_4$ and $MgFe_2O_4$ contents in $MgFe_2O_4$-phase could be caused by the reaction of $FeFeO_3$ (bridgmanite) = ¾ $Fe_{8/3}O_4$ ($MgFe_2O_4$-phase) or $MgFe_2O_4$ ($MgFe_2O_4$-phase) = ¾ $Fe_{8/3}O_4$ ($MgFe_2O_4$-phase) + MgO (periclase). The Mg_2SiO_4 content has a much smaller pressure dependence than the $Fe_{8/3}O_4$ content: it slightly decreases from 7–15 to 4–8 mol % with increasing pressure from 27 to 40 GPa (Table 1). These observations imply that the negative pressure dependence of Fe^{3+} content in bridgmanite is dominated by dissolution of Fe^{3+} from bridgmanite and formation of the $Fe_{8/3}O_4$ component in the $MgFe_2O_4$-phase, but the replacement of Fe^{3+} in bridgmanite by Mg^{2+} and Si^{4+} released from the $MgFe_2O_4$-phase also partially contributes to the decrease of Fe^{3+} in bridgmanite.

4.5. Implications for Chemistry of Fe^{3+}-Rich Bridgmanite

4.5.1. Fe^{3+}-Bearing and Al-Free System

Because bridgmanite coexists with ferropericlase and $MgFe_2O_4$-phase in the MgO-SiO_2-Fe_2O_3 ternary system under MgO-rich conditions, the experimentally determined $MgFeO_{2.5}$, $FeFeO_3$, and total Fe^{3+} contents should represent their maximum contents in Al-free bridgmanite when ferropericlase is present. Fei et al. (2020) demonstrated that the concentration of $FeFeO_3$ component increases with increasing temperature, whereas the $MgFeO_{2.5}$ content has no clear temperature dependence when bridgmanite coexists with ferropericlase at 27 GPa. On the other hand, the $MgFeO_{2.5}$, $FeFeO_3$, and total Fe^{3+} contents are found to decrease with increasing pressure in the present study (Figures 7a and 8a). By combining the pressure and temperature effects following the geotherm in the lower mantle (Katsura et al., 2010), the $MgFeO_{2.5}$ content in Al-free bridgmanite coexisting with

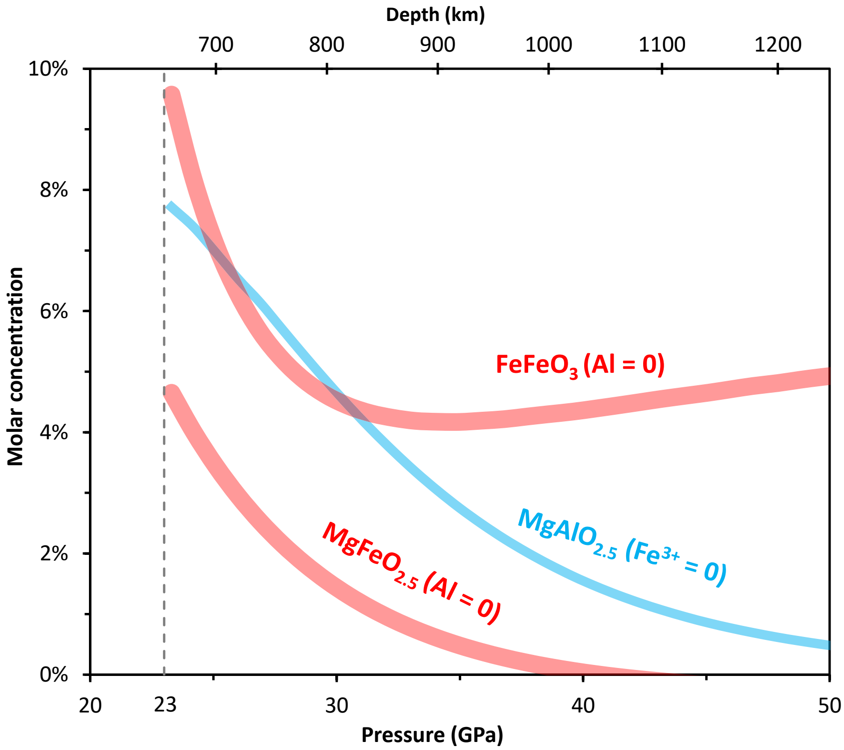

Figure 10. $FeFeO_3$ and $MgFeO_{2.5}$ contents as a function of depth according to the pressure dependences determined in this study, temperature dependences given by Fei et al. (2020), and geotherm from Katsura et al. (2010). The $MgAlO_{2.5}$ content in Fe^{3+}-free bridgmanite is based on the pressure and temperature dependences given by Liu, Ishii, and Katsura (2017) and Liu, Akaogi, & Katsura (2019).

ferropericlase decreases rapidly by more than two orders of magnitude from 4 to 5 mol % at the topmost lower mantle to nearly zero at 1,000–1,200 km depth. In contrast, the $FeFeO_3$ content decreases from 8% at 700 km depth to a minimum of ~4% at about 800 km depth, and is nearly constant or slightly increases to 5% at 1,200 km depth because of the negative and positive pressure and temperature dependences, respectively (Figure 10).

4.5.2. Fe^{3+} and Al-Bearing System

The pure Fe^{3+}-bearing (MgO-SiO_2-Fe_2O_3) system is ideal model for understanding the chemistry of bridgmanite. A more realistic approach for bridgmanite in the lower mantle considers both Fe^{3+} and Al^{3+} (e.g., Frost & McCammon, 2008; Irifune, 1994). The substitution mechanism will be controlled by the ratio of Al^{3+} and Fe^{3+} because of the formation of the $FeAlO_3$ component (e.g., Huang, Boffa-Ballaran, McCammon, Miyajima, Dolejš & Frost, 2021; Liu et al., 2020; Mohn & Trønnes, 2016; Richmond & Brodholt, 1998; Walter et al., 2006; Zhang & Oganov, 2006). When the Al^{3+}/Fe^{3+} atomic ratio is larger than unity, all Fe^{3+} will be consumed by the $FeAlO_3$ component, whereas excess Al^{3+} will form the $AlAlO_3$ and $MgAlO_{2.5}$ components (Huang, Boffa-Ballaran, McCammon, Miyajima, Dolejš & Frost, 2021; Huang, Boffa-Ballaran, McCammon, Miyajima, & Frost, 2021; Mohn & Trønnes, 2016). In contrast, when the Al^{3+}/Fe^{3+} ratio is smaller than unity, excess Fe^{3+} will form the $FeFeO_3$ and $MgFeO_{2.5}$ components in addition to the $FeAlO_3$ component (Huang, Boffa-Ballaran, McCammon, Miyajima, Dolejš & Frost, 2021; Mohn & Trønnes, 2016).

Although the Fe^{3+} content in bridgmanite under deep lower mantle conditions is considered to be relatively low in comparison with Al^{3+} (Frost & McCammon, 2008; Irifune & Ringwood, 1987a; Kurnosov et al., 2017; Lauterbach et al., 2000; Liu et al., 2020; Nakajima et al., 2012; Prescher et al., 2014; Shim et al., 2017; Sinmyo et al., 2019) and therefore Fe^{3+} should mainly form $FeAlO_3$, Fe^{3+}/Al^{3+} could be larger than unity in some regions. For example, bridgmanite in the topmost lower mantle has relatively high Fe^{3+} solubility (Fei et al., 2020; Liu et al., 2018; Wang et al., 2021) but low Al^{3+} solubility (Liu et al., 2016; Panero et al., 2006), subducted slabs may have relatively high oxygen fugacity conditions and thus should be Fe^{3+}-enriched (Zhao et al., 2021), and harzburgitic rocks are depleted in Al^{3+} (e.g., Irifune & Ringwood, 1987b). All of these regions may have relatively high Fe^{3+} content in bridgmanite, and thus $MgFeO_{2.5}$ and $FeFeO_3$ components could be formed. Their concentrations should decrease rapidly with increasing pressure because of the negative pressure dependence of their solubilities as determined in this study.

4.6. Implications for Lower Mantle Dynamics

The presence of $MgFeO_{2.5}$ and $FeFeO_3$ components in bridgmanite may affect its physical and chemical properties as predicted from the effects of $MgAlO_{2.5}$ and $AlAlO_3$ components (e.g., Andrault et al., 2001, 2007; Boffa-Ballaran et al., 2012; Brodholt, 2000; Daniel et al., 2004; Frost & Langenhorst, 2002; Saikia et al., 2009; Xu et al., 1998; Yagi et al., 2004; Zhang & Weidner, 1999). Because the $MgFeO_{2.5}$ component contains oxygen vacancies, the atomic diffusivity, which is proportional to the defect concentration, is expected to be enhanced. On the other hand, although the $FeFeO_3$ component does not produce vacancies, it should strongly distort the crystal structure of bridgmanite by substitution of Fe^{3+} on the Si site compared to other components such as $MgSiO_3$, $AlAlO_3$, $FeSiO_3$, and $FeAlO_3$ due to the much larger ionic radius of Fe^{3+} compared to Si^{4+} and Al^{3+}. As a result, the $FeFeO_3$ component is expected to enhance element diffusivities as well. Therefore, the decrease of both $FeFeO_3$ and $MgFeO_{2.5}$ content with pressure may cause decreasing atomic diffusivities in bridgmanite, which may affect diffusion-controlled physical and chemical processes and thus affect the mantle dynamics.

One example is mantle rheology. The creep of minerals is controlled by diffusion of the slowest species (e.g., Herring, 1950; Nabarro, 1967). Although the viscosity of bridgmanite is controlled by Mg and Si diffusion rather than O because Mg and Si diffuse slower than O (e.g., Dobson et al., 2008; Holzapfel et al., 2005; Xu et al., 2011; Yamazaki et al., 2000), both Mg and Si are fully surrounded by O in polyhedrons. The hopping of Mg and Si ions from/into the polyhedron should become easier when an oxygen ion is missing. Hence, oxygen vacancies may enhance the diffusion of Mg and Si and thus reduce the viscosity. Therefore, it is predicted that the decrease in both $FeFeO_3$ and $MgFeO_{2.5}$ contents in bridgmanite from 700 to ∼1,000–1,200 km depth could suppress Mg and Si diffusivities in bridgmanite, which may contribute to the large viscosity increase in the midmantle inferred from geoid analysis (Rudolph et al., 2015).

Another example is electrical conductivity in the lower mantle. The electrical conductivity of bridgmanite is dominated by the ionic conduction mechanism at relatively high temperatures (e.g., Dobson, 2003; Xu & McCammon, 2002; Yoshino et al., 2016), which is controlled by atomic diffusion of the fastest species, that is, O in bridgmanite (Dobson et al., 2008). Therefore, based on the Nernst-Einstein relation, the ionic conductivity of bridgmanite should be enhanced by the presence of the $MgFeO_{2.5}$ component. The decreasing of $MgFeO_{2.5}$ content with depth may contribute to the decrease in observed conductivity at >800 km depth based on magnetotelluric sounding (e.g., Civet et al., 2015; Civet & Tarits, 2013).

The above examples are based on qualitative interpretation. To constrain the role of $MgFeO_{2.5}$ and $FeFeO_3$ components on mantle dynamics in more detail, further investigations about their effects on the physical and chemical properties of bridgmanite are required. Additionally, as mentioned above, bridgmanite in the lower mantle contains Al^{3+}, which could affect the substitution mechanism of Fe^{3+} (e.g., Huang, Boffa-Ballaran, McCammon, Miyajima, Dolejš & Frost, 2021; Huang, Boffa-Ballaran, McCammon, Miyajima, & Frost, 2021; Liu et al., 2020). More experimental studies on the pressure and temperature dependences of Fe^{3+} substitution in both Fe^{3+} and Al^{3+} bearing bridgmanite are therefore necessary following the pattern of the detailed investigated in Huang, Boffa-Ballaran, McCammon, Miyajima, Dolejš and Frost (2021); Huang, Boffa-Ballaran, McCammon, Miyajima, and Frost (2021); at a single condition (25 GPa, 1970 K) corresponding to the topmost lower mantle.

Data Availability Statement

The EPMA, XRD, and Mössbauer data for this paper are given in Zenodo (https://doi.org/10.5281/zenodo.5661686).

Acknowledgments

We acknowledge the European Research Council (ERC) research Grant (No. 787527) and the Deutsche Forschungsgemeinschaft (DFG) (KA3434/9-1, KA3434/11-1, KA3434/12-1) to T. Katsura, and the annual budget of Bayerisches Geoinstitut to H. Fei for financial support to this study. The Synchrotron Mossbauer source spectroscopy analysis was performed with the approval of the Japan Synchrotron Radiation Research Institute (2019B1136). Open access funding enabled and organized by Projekt DEAL.

References

Andrault, D., & Bolfan-Casanova, N. (2001). High-pressure phase transformations in the $MgFe_2O_4$ and Fe_2O_3-$MgSiO_3$ systems. *Physics and Chemistry of Minerals*, *28*, 211–217. https://doi.org/10.1007/s002690000149

Andrault, D., Bolfan-Casanova, N., Bouhifd, M. A., Guignot, N., & Kawamoto, T. (2007). The role of Al-defects on the equation of state of Al-(Mg,Fe)SiO_3 perovskite. *Earth and Planetary Science Letters*, *263*, 167–179. https://doi.org/10.1016/j.epsl.2007.08.012

Andrault, D., Bolfan-Casanova, N., & Guignot, N. (2001). Equation of state of lower mantle (Al,Fe)-MgSiO3 perovskite. *Earth and Planetary Science Letters*, *193*, 501–508. https://doi.org/10.1016/s0012-821x(01)00506-4

Andrault, D., Munoz, M., Pesce, G., Cerantola, V., Chumakov, A., Kantor, I., et al. (2018). Large oxygen excess in the primitive mantle could be the source of the great oxygenation event. *Geochemical Perspectives Letters*, *6*, 5–10. https://doi.org/10.7185/geochemlet.1801

Andrault, D., Neuville, D. R., Flank, A. M., & Wang, Y. (1998). Cation sites in Al-rich $MgSiO_3$ perovskites. *American Mineralogist*, *83*, 1045–1053. https://doi.org/10.2138/am-1998-9-1013

Armstrong, K., Frost, D., McCammon, C. A., Rubie, D. C., & Boffa-Ballaran, T. (2019). Deep magma ocean formation set the oxidation state of Earth's mantle. *Science*, *365*, 903–906. https://doi.org/10.1126/science.aax8376

Bindi, L., Shim, S. H., Sharp, T. G., & Xie, X. (2020). Evidence for the charge disproportionation of iron in extraterrestrial bridgmanite. *Science Advances*, *6*, eaay7893. https://doi.org/10.1126/sciadv.aay7893

Boffa-Ballaran, T., Kurnosov, A., Glazyrin, K., Frost, D. J., Merlin, M., Hanfland, M., & Caracas, R. (2012). Effect of chemistry on the compressibility of silicate perovskite in the lower mantle. *Earth and Planetary Science Letters*, *333*, 181–190. https://doi.org/10.1016/j.epsl.2012.03.029

Boujibar, A., Bolfan-Casanova, N., Andrault, D., Bouhifd, M. A., & Tracera, N. (2016). Incorporation of Fe^{2+} and Fe^{3+} in bridgmanite during magma ocean crystallization. *American Mineralogist*, *101*, 1560–1570. https://doi.org/10.2138/am-2016-5561

Brodholt, J. P. (2000). Pressure-induced changes in the compression mechanism of aluminous perovskite in the Earth's mantle. *Nature*, *407*, 620–622. https://doi.org/10.1038/35036565

Catalli, K., Shim, S. H., Prakapenka, V. B., Zhao, J., Sturhahn, W., Chow, P., et al. (2010). Spin state of ferric iron in $MgSiO_3$ perovskite and its effect on elastic properties. *Earth and Planetary Science Letters*, *289*, 68–75. https://doi.org/10.1016/j.epsl.2009.10.029

Civet, F., & Tarits, P. (2013). Analysis of magnetic satellite data to infer the mantle electrical conductivity of telluric planets in the solar system, Planet. *Space Science*, *84*, 102–111. https://doi.org/10.1016/j.pss.2013.05.004

Civet, F., Thebault, E., Verhoeven, O., Langlais, B., & Saturnino, D. (2015). Electrical conductivity of the Earth's mantle from the first Swarm magnetic field measurements. *Geophysical Research Letters*, *42*, 3338–3346. https://doi.org/10.1002/2015GL063397

Creasy, N., Girard, J. J. O. E., Jr., & Lee, K. K. M. (2020). The role of redox on bridgmanite crystal chemistry and calcium speciation in the lower mantle. *Journal of Geophysical Research*, *125*, e2020JB020783. https://doi.org/10.1029/2020JB020783

Daniel, I., Bass, J. D., Fiquet, G., Cardon, H., Zhang, J., & Hanfland, M. (2004). Effect of aluminium on the compressibility of silicate perovskite. *Geophysical Research Letters*, *31*, L15608. https://doi.org/10.1029/2004GL020213

Dewaele, A., & Torrent, M. (2013). Equation of state of α-Al_2O_3. *Physical Review B: Condensed Matter*, *88*, 064107. https://doi.org/10.1103/physrevb.88.064107

Dobson, D. P. (2003). Oxygen ionic conduction in $MgSiO_3$ perovskite. *Physics of the Earth and Planetary Interiors*, *139*, 55–64. https://doi.org/10.1016/s0031-9201(03)00144-4

Dobson, D. P., Dohmen, R., & Wiedenbeck, M. (2008). Self-diffusion of oxygen and silicon in $MgSiO_3$ perovskite. *Earth and Planetary Science Letters*, *270*, 125–129. https://doi.org/10.1016/j.epsl.2008.03.029

Dorogokupets, P. L. (2010). P-V-T equations of state of MgO and thermodynamics. *Physics and Chemistry of Minerals*, *37*, 677–684. https://doi.org/10.1007/s00269-010-0367-2

Fei, H., Liu, Z. D., McCammon, C. A., & Katsura, T. (2020). Oxygen vacancy substitution linked to ferric iron in bridgmanite at 27 GPa. *Geophysical Research Letters*, *47*, e2019GL086296. https://doi.org/10.1029/2019GL086296

Fei, Y., Virgo, D., Mysen, B. O., Wang, Y., & Mao, H. K. (1994). Temperature dependent electron delocalization in (Mg,Fe)SiO_3 perovskite. *American Mineralogist*, *79*, 826–837.

Frost, D., & Langenhorst, F. (2002). The effect of Al_2O_3 on Fe-Mg partitioning between magnesiowüstite and magnesium silicate perovskite. *Earth and Planetary Science Letters*, *199*, 227–241. https://doi.org/10.1016/s0012-821x(02)00558-7

Frost, D., Liebske, C., Langenhorst, F., McCammon, C. A., Tronnes, R. G., & Rubie, D. C. (2004). Experimental evidence for the existence of iron-rich metal in the Earth's lower mantle. *Nature*, *428*, 409–412. https://doi.org/10.1038/nature02413

Frost, D., Mann, U., Asahara, Y., & Rubie, D. C. (2008). The redox state of the mantle during and just after core formation. *Philosophical Transactions of the Royal Society A*, *366*, 4315–4337. https://doi.org/10.1098/rsta.2008.0147

Frost, D., & McCammon, C. A. (2008). The redox state of Earth's mantle. *Annual Review of Earth and Planetary Sciences*, *36*, 389–420. https://doi.org/10.1146/annurev.earth.36.031207.124322

Glazyrin, K., Boffa-Ballaran, T., Frost, D. J., McCammon, C., Kantor, A., Merlini, M., et al. (2014). Magnesium silicate perovskite and effect of iron oxidation state on its bulk sound velocity at the conditions of the lower mantle. *Earth and Planetary Science Letters*, *393*, 182–186. https://doi.org/10.1016/j.epsl.2014.01.056

Greenberg, E., Xu, W. M., Nikolaevsky, M., Bykova, E., Garbarino, G., Glazyrin, K., et al. (2017). High-pressure magnetic, electronic, and structural properties of MFe_2O_4 (M = Mg,Zn,Fe) ferric spinels. *Physical Review B*, *95*(19), 195150. https://doi.org/10.1103/physrevb.95.195150

Grocholski, B., Shim, S. H., Sturhahn, W., Zhao, J., Xiao, Y., & Chow, P. C. (2009). Spin and valence states of iron in $(Mg_{0.8}Fe_{0.2})SiO_3$ perovskite. *Geophysical Research Letters*, *36*, L24303. https://doi.org/10.1029/2009GL041262

Grüninger, H., Liu, Z., Siegel, R., Boffa-Ballaran, T., Katsura, T., Senker, J., & Frost, D. J. (2019). Oxygen vacancy ordering in aluminous bridgmanite in the Earth's lower mantle. *Geophysical Research Letters*, *46*, 8731–8740. https://doi.org/10.1029/2019GL083613

Gu, T., Li, M., McCammon, C., & Lee, K. K. M. (2016). Redox-induced lower mantle density contrast and effect on mantle structure and primitive oxygen. *Nature Geoscience*, *9*, 723–727. https://doi.org/10.1038/ngeo2772

Herring, C. (1950). Diffusional viscosity of a polycrystalline solid. *Journal of Applied Physics*, *21*, 437–445. https://doi.org/10.1063/1.1699681

Hirao, N., Kawaguchi, S. I., Hirose, K., Shimizu, K., Ohtani, E., & Ohishi, Y. (2020). New developments in high-pressure X-ray diffraction beamline for diamond anvil cell at Spring-8. *Matter and Radiation at Extremes*, *5*, 018403. https://doi.org/10.1063/1.5126038

Holzapfel, C., Rubie, D. C., Frost, D. J., & Langenhorst, F. (2005). Fe-Mg interdiffusion in (Mg,Fe)SiO_3 perovskite and lower mantle reequilibration. *Science*, *309*, 1707–1710. https://doi.org/10.1126/science.1111895

Hu, Q., Kim, D. Y., Yang, W., Yang, L., Meng, Y., Zhang, L., & Mao, H. K. (2016). FeO_2 and FeOOH under deep lower-mantle conditions and Earth's oxygen-hydrogen cycles. *Nature*, *534*, 241–244. https://doi.org/10.1038/nature18018

Huang, R. (2020). *Bridgmanite crystal chemistry and iron content in the Earth's lower mantle* (Ph.D. dissertation, p. 212). The University of Bayreuth. https://doi.org/10.15495/EPub_UBT_00004611

Huang, R., Boffa-Ballaran, T., McCammon, C. A., Miyajima, N., Dolejš, D., & Frost, D. J. (2021). The composition and redox state of bridgmanite in the lower mantle as a function of oxygen fugacity. *Geochimica et Cosmochimica Acta*, *303*, 110–136. https://doi.org/10.1016/j.gca.2021.02.036

Huang, R., Boffa-Ballaran, T., McCammon, C. A., Miyajima, N., & Frost, D. J. (2021). The effect of Fe-Al substitution on the crystal structure of $MgSiO_3$ bridgmanite. *Journal of Geophysical Research*, *126*, e2021JB021936. https://doi.org/10.1029/2021JB021936

Hummer, D. R., & Fei, Y. (2012). Synthesis and crystal chemistry of Fe^{3+}-bearing $(Mg,Fe^{3+})(Si,Fe^{3+})O_3$ perovskite. *American Mineralogist*, *97*, 1915–1921. https://doi.org/10.2138/am.2012.4144

Irifune, T. (1994). Absence of an aluminous phase in the upper part of the Earth's lower mantle. *Nature*, *370*, 131–133. https://doi.org/10.1038/370131a0

Irifune, T., & Ringwood, A. E. (1987a). Phase transformations in primitive MORB and pyrolite compositions to 25 GPa and some geophysical implications. *Geophysical Monograph Series*, 231, 242, https://doi.org/10.1029/GM039p0231

Irifune, T., & Ringwood, A. E. (1987b). Phase transformations in a harzburgite composition to 26 GPa: Implications for dynamical behavior of the subducting slab. *Earth and Planetary Science Letters*, *86*, 365–376. https://doi.org/10.1016/0012-821x(87)90233-0

Ishii, T., Huang, R., Fei, H., Koemets, I., Liu, Z., Maeda, F., et al. (2018). Complete agreement of the post-spinel transition with 660-km seismic discontinuity. *Scientific Reports*, *8*, 6358. https://doi.org/10.1038/s41598-018-24832-y

Ishii, T., Liu, Z., & Katsura, T. (2019). A breakthrough in pressure generation by a Kawai-type multi-anvil apparatus with tungsten carbide anvils. *Engineering*, *5*, 434–440. https://doi.org/10.1016/j.eng.2019.01.013

Ishii, T., Miyajima, N., Sinmyo, R., Kojitani, H., Mori, D., Inaguma, Y., & Akaogi, M. (2020). Discovery of new-structured post-spinel $MgFe_2O_4$: Crystal structure and high-pressure phase relations. *Geophysical Research Letters*, *47*, e2020GL087490. https://doi.org/10.1029/2020GL087490

Ishii, T., Shi, L., Huang, R., Tsujino, N., Druzhbin, D., Myhill, R., et al. (2016). Generation of pressures over 40 GPa using Kawai-type multi-anvil press with tungsten carbide anvils. *Review of Scientific Instruments*, *87*, 024501. https://doi.org/10.1063/1.4941716

Jackson, J. M., Sturhahn, W., Shen, G., Zhao, J., Hu, M. Y., Errandonea, D., et al. (2005). A synchrotron Mössbauer spectroscopy study of $(Mg,Fe)SiO_3$ perovskite up to 120 GPa. *American Mineralogist*, *90*, 199–205. https://doi.org/10.2138/am.2005.1633

Katsura, T., Yoneda, A., Yamazaki, D., Yoshino, T., & Ito, E. (2010). Adiabatic temperature profile in the mantle. *Physics of the Earth and Planetary Interiors*, *183*, 212–218. https://doi.org/10.1016/j.pepi.2010.07.001

Kojitani, H., Hisatomi, R., & Akaogi, M. (2007). High-pressure phase relations and crystal chemistry of calcium ferrite-type solid solutions in the system $MgAl_2O_4$-Mg_2SiO_4. *American Mineralogist*, *92*, 1112–1118. https://doi.org/10.2138/am.2007.2255

Kojitani, H., Katsura, T., & Akaogi, M. (2007). Aluminum substitution mechanisms in perovskite-type $MgSiO_3$: An investigation by Rietveld analysis. *Physics and Chemistry of Minerals*, *34*, 257–267. https://doi.org/10.1007/s00269-007-0144-z

Kupenko, I., McCammon, C., Sinmyo, R., Cerantola, V., Potapkin, V., Chumakov, A. I., et al. (2015). Oxidation state of the lower mantle: In situ observations of the iron electronic configuration in bridgmanite at extreme conditions. *Earth and Planetary Science Letters*, *423*, 78–86. https://doi.org/10.1016/j.epsl.2015.04.027

Kurnosov, A., Marquardt, H., Frost, D. J., Boffa-Ballaran, T., & Ziberna, L. (2017). Evidence for a Fe^{3+}-rich pyrolitic lower mantle from (Al,Fe)-bearing bridgmanite elasticity data. *Nature*, *543*, 543–546. https://doi.org/10.1038/nature21390

Lauterbach, S., McCammon, C. A., van Aken, P., Langenhorst, F., & Seifert, F. (2000). Mössbauer and ELNES spectroscopy of $(Mg,Fe)(Si,Al)O_3$ perovskite: A highly oxidised component of the lower mantle. *Contributions to Mineralogy and Petrology*, *138*, 17–26. https://doi.org/10.1007/PL00007658

Li, J., Sturhahn, W., Jackson, J. M., Struzhkin, V. V., Lin, J. F., Zhao, J., et al. (2006). Pressure effect on the electronic structure of iron in $(Mg,Fe)(Si,Al)O_3$ perovskite: A combined synchrotron Mössbauer and X-ray emission spectroscopy study up to 100 GPa. *Physics and Chemistry of Minerals*, *33*, 575–585. https://doi.org/10.1007/s00269-006-0105-y

Liu, J., Dorfam, S. M., Zhu, F., Li, J., Wang, Y., Zhang, D., et al. (2018). Valence and spin states of iron are invisible in Earth's lower mantle. *Nature Communications*, *9*, 1284. https://doi.org/10.1038/s41467-018-03671-5

Liu, Z., Akaogi, M., & Katsura, T. (2019). Increase of the oxygen vacancy component in bridgmanite with temperature. *Earth and Planetary Science Letters*, *505*, 141–151. https://doi.org/10.1016/j.epsl.2018.10.014

Liu, Z., Boffa-Ballaran, T., Huang, R., Frost, D., & Katsura, T. (2019). Strong correlation of oxygen vacancies in bridgmanite with Mg/Si ratio. *Earth and Planetary Science Letters*, *523*, 115697. https://doi.org/10.1016/j.epsl.2019.06.037

Liu, Z., Dubrovinsky, L., McCammon, C. A., Ovsyanikov, S. V., Koemets, I., Chen, L., et al. (2019). A new $(Mg_{0.5}Fe_{0.5}{}^{3+})(Si_{0.5}Al_{0.5}{}^{3+})O_3$ $LiNbO_3$-type phase synthesized at lower mantle conditions. *American Mineralogist*, *104*, 1213–1216. https://doi.org/10.2138/am-2019-7070

Liu, Z., Irifune, T., Nishi, M., Tange, Y., Arimoto, T., & Shinmei, T. (2016). Phase relations in the system $MgSiO_3$–Al_2O_3 up to 52 GPa and 2000 K. *Physics of the Earth and Planetary Interiors*, *257*, 18–27. https://doi.org/10.1016/j.pepi.2016.05.006

Liu, Z., Ishii, T., & Katsura, T. (2017). Rapid decrease of $MgAlO_{2.5}$ component in bridgmanite with pressure. *Geochemical Perspectives Letters*, *5*, 12–18. https://doi.org/10.7185/geochemlet.1739

Liu, Z., McCammon, C., Wang, B., Dubrovinsky, L., Ishii, T., Bondar, D., et al. (2020). Stability and solubility of the $FeAlO_3$ component in bridgmanite at uppermost lower mantle conditions. *Journal of Geophysical Research*, *125*, e2019JB018447. https://doi.org/10.1029/2019JB018447

Liu, Z., Nishi, M., Ishii, T., Fei, H., Miyajima, N., Boffa-Ballaran, T., et al. (2017). Phase relations in the system $MgSiO_3$-Al_2O_3 up to 2300 K at lower mantle pressures. *Journal of Geophysical Research*, *122*, 7775–7788. https://doi.org/10.1002/2017JB014579

McCammon, C. A. (1997). Perovskite as a possible sink for ferric iron in the lower mantle. *Nature*, *387*, 694–696. https://doi.org/10.1038/42685

McCammon, C. A. (1998). The crystal chemistry of ferric iron in $Mg_{0.05}Fe_{0.95}SiO_3$ perovskite as determined by Mössbauer spectroscopy in the temperature range 80-293 K. *Physics and Chemistry of Minerals*, *25*, 292–300. https://doi.org/10.1007/s002690050117

Mohn, C. E., & Trønnes, R. G. (2016). Iron spin state and site distribution in $FeAlO_3$-bearing bridgmanite. *Earth and Planetary Science Letters*, *440*, 178–186. https://doi.org/10.1016/j.epsl.2016.02.010

Murakami, M., Hirose, K., Kawamura, K., Sata, N., & Ohishi, Y. (2004). Post-perovskite phase transition in $MgSiO_3$. *Science*, *304*, 855–858. https://doi.org/10.1126/science.1095932

Nabarro, F. R. N. (1967). Steady-state diffusion creep. *Philosophical Magazine*, *16*, 231–237. https://doi.org/10.1080/14786436708229736

Nakajima, Y., Frost, D. J., & Rubie, D. C. (2012). Ferrous iron partitioning between magnesium silicate perovskite and ferropericlase and the composition of perovskite in the Earth's lower mantle. *Journal of Geophysical Research*, *117*, B08201. https://doi.org/10.1029/2012JB009151

Navrotsky, A. (1999). A lesson from ceramics. *Science*, *284*, 1788–1789. https://doi.org/10.1126/science.284.5421.1788

Navrotsky, A., Schoenitz, M., Kojitani, H., Xu, H., Zhang, J., Weidner, D. J., & Jeanloz, R. (2003). Aluminum in magnesium silicate perovskite: Formation, structure, and energetics of magnesium-rich defect solid solutions. *Journal of Geophysical Research*, *108*(B7), 2330. https://doi.org/10.1029/2002JB002055

Nishio-Hamane, D., Nagai, T., Fujino, K., Seto, Y., & Takafuji, N. (2005). Fe^{3+} and Al solubilities in $MgSiO_3$ perovskite: Implication of the Fe^{3+}AlO3 substitution in $MgSiO_3$ perovskite at the lower mantle condition. *Geophysical Research Letters*, *32*, L16306. https://doi.org/10.1029/2005GL023529

Nishio-Hamane, D., Seto, Y., Fujino, K., & Nagai, T. (2008). Effect of $FeAlO_3$ incorporation into $MgSiO_3$ on the bulk modulus of perovskite. *Physics of the Earth and Planetary Interiors*, *166*, 219–225. https://doi.org/10.1016/j.pepi.2008.01.002

O'Neill, B., & Jeanloz, R. (1994). $MgSiO_3$-$FeSiO_3$-Al_2O_3 in the Earth's lower mantle: Perovskite and garnet at 1200 km depth. *Journal of Geophysical Research*, *99*, 19901–19915. http://doi.org/10.1029/94jb01752

Panero, W. R., Akber-Knutson, S., & Stixrude, L. (2006). Al_2O_3 incorporation in $MgSiO_3$ perovskite and ilmenite. *Earth and Planetary Science Letters*, *252*, 152–161. https://doi.org/10.1016/j.epsl.2006.09.036

Piet, H., Badro, J., Nabiei, F., Dennenwaldt, T., Shim, S. H., Cantoni, M., et al. (2016). Spin and valence dependence of iron partitioning in Earth's deep mantle. *Proceedings of the National Academy of Sciences of the United States of America*, *113*, 11127–11130. https://doi.org/10.1073/pnas.1605290113

Prescher, C., Langenhorst, F., Dubrovinsky, L. S., Prakapenka, V. B., & Miyajima, N. (2014). The effect of Fe spin crossovers on its partitioning behavior and oxidation state in a pyrolitic Earth's lower mantle system. *Earth and Planetary Science Letters*, *399*, 86–91. https://doi.org/10.1016/j.epsl.2014.05.011

Prescher, C., McCammon, C., & Dubrovinsky, L. (2012). MossA: A program for analyzing energy-domain Mössbauer spectra from conventional and synchrotron sources. *Journal of Applies Crystallography*, *45*, 329–331. https://doi.org/10.1107/s0021889812004979

Richmond, N. C., & Brodholt, J. P. (1998). Calculated role of aluminium in the incorporation of ferric iron into magnesium silicate perovskite. *American Mineralogist*, *83*, 947–951. https://doi.org/10.2138/am-1998-9-1003

Rudolph, M. L., Lekic, V., & Lithgow-Bertelloni, C. (2015). Viscosity jump in Earth's mid-mantle. *Science*, *350*, 1349–1352. https://doi.org/10.1126/science.aad1929

Saikia, A., Boffa-Ballaran, T., & Frost, D. J. (2009). The effect of Fe and Al substitution on the compressibility of $MgSiO_3$-perovskite determined through single-crystal X-ray diffraction. *Physics of the Earth and Planetary Interiors*, *173*, 153–161. https://doi.org/10.1016/j.pepi.2008.11.006

Shim, S. H., Grocholski, B., Ye, Y., Alp, E. E., Xu, S., Morgan, D., et al. (2017). Stability of ferrous-iron-rich bridgmanite under reducing midmantle conditions. *Proceedings of the National Academy of Sciences of the United States of America*, *114*(25), 6468–6473. https://doi.org/10.1073/pnas.1614036114

Sinmyo, R., Bykova, E., McCammon, C., Kupenko, I., Potapkin, V., & Dubrovinsky, L. (2014). Crystal chemistry of Fe^{3+}-bearing (Mg, Fe) SiO_3 perovskite: A single-crystal X-ray diffraction study. *Physics and Chemistry of Minerals*, *41*, 409–417. https://doi.org/10.1007/s00269-013-0639-8

Sinmyo, R., Hirose, K., Muto, S., Ohishi, Y., & Yasuhara, A. (2011). The valence state and partitioning of iron in the Earth's lowermost mantle. *Journal of Geophysical Research*, *116*, B07205. https://doi.org/10.1029/2010JB008179

Sinmyo, R., Nakajima, Y., McCammon, C., Miyajima, N., Petitgirard, S., Myhill, R., et al. (2019). Effect of Fe^{3+} on phase relations in the lower mantle: Implications for redox melting in stagnant slabs. *Journal of Geophysical Research*, *124*, 12484–12497. https://doi.org/10.1029/2019JB017704

Stebbins, J. F., Kojitani, H., Akaogi, M., & Navrotsky, A. (2003). Aluminum substitution in $MgSiO_3$ perovskite: Investigation of multiple mechanisms by ^{27}Al NMR. *American Mineralogist*, *88*, 1161–1164. https://doi.org/10.2138/am-2003-0724

Sueda, Y., Irifune, T., Sanehira, T., Yagi, T., Nishiyama, N., Kikegawa, T., & Funakoshi, K. I. (2009). Thermal equation of state of $CaFe_2O_4$-type $MgAl_2O_4$. *Physics of the Earth and Planetary Interiors*, *174*, 78–85. https://doi.org/10.1016/j.pepi.2008.07.046

Tange, Y., Kuwayama, Y., Irifune, T., Funakoshi, K. I., & Ohishi, Y. (2012). P-V-T equation of state of $MgSiO_3$ perovskite based on the MgO pressure scale: A comprehensive reference for mineralogy of the lower mantle. *Journal of Geophysical Research*, *117*, B06201. https://doi.org/10.1029/2011jb008988

Uenver-Thiele, L., Woodland, A. B., Boffa-Ballaran, T., Miyajima, N., & Frost, D. J. (2017). Phase relations of Fe-Mg spinels including new high-pressure post-spinel phases and implications for natural samples. *American Mineralogist*, *102*, 2054–2064. https://doi.org/10.2138/am-2017-6119

Vanpeteghem, C. B., Angel, R. J., Ross, N. L., Jacobsen, S. D., Dobson, D. P., Litasov, K. D., & Ohtani, E. (2006). Al, Fe substitution in the $MgSiO_3$ perovskite structure: A single-crystal X-ray diffraction study. *Physics of the Earth and Planetary Interiors*, *155*, 96–103. https://doi.org/10.1016/j.pepi.2005.10.003

Walter, M. J., Kubo, A., Yoshino, T., Brodholt, J., Koga, K. T., & Ohishi, Y. (2004). Phase relations and equation-of-state of aluminous Mg-silicate perovskite and implications for Earth's lower mantle Earth Planet. *Science Letter*, *222*, 501–516. https://doi.org/10.1016/j.epsl.2004.03.014

Walter, M. J., Trønnes, R. G., Armstrong, L. S., Lord, O. T., Caldwell, W. A., & Clark, S. M. (2006). Subsolidus phase relations and perovskite compressibility in the system MgO-$AlO_{1.5}$-SiO_2 with implications for Earth's lower mantle. *Earth and Planetary Science Letters*, *248*, 77–89. https://doi.org/10.1016/j.epsl.2006.05.017

Wang, W., Liu, J., Zhu, F., Li, M., Dorfman, S. M., Li, J., & Wu, Z. (2021). Formation of large low shear velocity provinces through the decomposition of oxidized mantle. *Nature Communications*, *12*, 1911. https://doi.org/10.1038/s41467-021-22185-1

Xu, J., Yamazaki, D., Katsura, T., Wu, X., Remmert, P., Yurimoto, H., & Chakraborty, S. (2011). Silicon and magnesium diffusion in a single crystal of $MgSiO_3$ perovskite. *Journal of Geophysical Research*, *116*, B12205. https://doi.org/10.1029/2011JB008444

Xu, S., Lin, J. F., & Morgan, D. (2017). Iron partitioning between ferropericlase and bridgmanite in the Earth's lower mantle. *Journal of Geophysical Research*, *122*, 1074–1087. https://doi.org/10.1002/2016JB013543

Xu, Y., & McCammon, C. (2002). Evidence for ionic conductivity in lower mantle $(Mg,Fe)(Si,Al)O_3$ perovskite. *Journal of Geophysical Research*, *107*(B10), 2251. https://doi.org/10.1029/2001JB000677

Xu, Y., McCammon, C., & Poe, B. T. (1998). The effect of alumina on the electrical conductivity of silicate perovskite. *Science*, *282*, 922–924. https://doi.org/10.1126/science.282.5390.922

Yagi, T., Okabe, K., Nishiyama, N., Kubo, A., & Kikegawa, T. (2004). Complicated effects of aluminum on the compressibility of silicate perovskite. *Physics of the Earth and Planetary Interiors*, *143*, 81–91. https://doi.org/10.1016/j.pepi.2003.07.020

Yamamoto, T., Yuen, D. A., & Ebisuzaki, T. (2003). Substitution mechanism of Al ions in $MgSiO_3$ perovskite under high pressure conditions from first-principles calculations. *Earth and Planetary Science Letters*, *206*, 617–625. https://doi.org/10.1016/s0012-821x(02)01099-3

Yamazaki, D., Kato, T., Yurimoto, H., Ohtani, E., & Toriumi, M. (2000). Silicon self-diffusion in $MgSiO_3$ perovskite at 25 GPa. *Physics of the Earth and Planetary Interiors*, *119*, 299–309. https://doi.org/10.1016/s0031-9201(00)00135-7

Yoshino, T., Kamada, S., Zhao, C., Ohtani, E., & Hirao, N. (2016). Electrical conductivity model of Al-bearing bridgmanite with implications for the electrical structure of the Earth's lower mantle. *Earth and Planetary Science Letters*, *434*, 208–219. https://doi.org/10.1016/j.epsl.2015.11.032

Zhang, F., & Oganov, A. R. (2006). Valence state and spin transitions of iron in Earth's mantle silicates. *Earth and Planetary Science Letters*, *249*, 436–443. https://doi.org/10.1016/j.epsl.2006.07.023

Zhang, J., & Weidner, D. J. (1999). Thermal equation of state of aluminum-enriched silicate perovskite. *Science*, *284*, 782–784. https://doi.org/10.1126/science.284.5415.782

Zhao, C., Yoshino, T., & Zhang, B. (2021). Oxidation extent of the upper mantle by subducted slab and possible oxygen budget in deep Earth inferred from redox kinetics of olivine. *ESSoAr*. https://doi.org/10.1002/essoar.10507782.1

Zhu, S., Liu, J., Hu, Q., Mao, W. L., Meng, Y., Zhang, D., et al. (2019). Structure-controlled oxygen concentration in Fe_2O_3 and FeO_2. *Inorganic Chemistry*, *58*, 5476–5482. https://doi.org/10.1021/acs.inorgchem.8b02764